In-Motion Initial Alignment Method Based on Vector Observation and Truncated Vectorized *K*-matrix for SINS

Haoqian Huang, *Member*, *IEEE*, Jiaying Wei, Di Wang, Li Zhang, *Senior Member*, *IEEE*, and Bing Wang, *Member*, *IEEE*

***Abstract*—In this paper, an improved in-motion coarse alignment method is proposed for the strapdown inertial navigation system (SINS) aided by the global positioning system (GPS). Traditional in-motion alignment methods suffer from complex noises contained in the outputs of inertial sensors and GPS. To solve this problem, this paper proposes an in-motion coarse alignment method using the vector observation and truncated vectorized *K*-matrix (VO-TVK) for autonomous underwater vehicles. The contributions of this study are twofold. Firstly, a new simplified model can be applied to the in-motion alignment process by employing the zero-trace and symmetry of the *K*-matrix. Secondly, the proposed VO-TVK algorithm can make up for the Optimal-REQUEST algorithm's drawbacks, where the Optimal-REQUEST algorithm has the conservative covariance matrix and the scalar gain. The simulation, vehicle test and lake trial results illustrate that the proposed VO-TVK algorithm can efficiently reduce the effects of noises contained in the vector observation and achieve better accuracy than the compared algorithms.**

***Index Terms*— Autonomous underwater vehicle, in-motion coarse alignment, Kalman filter, vector observation, Strapdown inertial navigation system**

I. INTRODUCTION

Autonomous underwater vehicles (AUV)s have been playing an increasingly important role in underwater missions, as it has excellent concealment and can replace humans to perform dangerous tasks [1]-[2]. Precise positioning and navigation capabilities are the keys to ensuring AUV completes the mission well [3]-[5]. Strapdown inertial navigation systems (SINS)s have been widely used in the field of navigation and positioning because it does not rely on external signal and is less susceptible to outside interference [6]-[8]. However, the performance of SINS highly depends on the accuracy of the initial navigation parameters, such as initial velocity, position and attitude [9]-[10]. Acquiring the initial information of SINS is typically called alignment, the SINS should firstly complete its alignment process before it steps into the steady working period [11]. Initial velocity and position can be directly obtained from external references like the global positioning system (GPS) and the Doppler velocity log (DVL) [12]. However, obtaining the initial attitude remains the dominant factor which influences accuracy of navigation [13]. The initial alignment process consists of the coarse alignment period and fine alignment period [14]. The former alignment period plays a necessary and preliminary part in the whole navigation mission, which estimates and provides a rough attitude estimation for the fine alignment [15].

A plenty of researchers devote themselves to developing new coarse alignment methods. It is worth noting the apparent motion of gravity in the inertial system can be described as a cone, using the center of the earth as the vertex. Based on that, a series of coarse alignment methods, which use the gravity in the inertial frame as a reference, have been investigated. Ref [16] employs the TRIAD algorithm to calculate the initial attitude based on the two vectors directly obtained by the accelerometers and gyroscopes. Ref [17] utilizes the Q-Method to calculate the initial attitude matrix, which is similar to the method proposed in Ref [16]. However, these self-alignment methods are only suitable for the swaying base or stationary base. In some cases, the TRIAD algorithm is limited when AUV needs to perform coarse alignment on moving base. Thus, Ref [18] innovatively proposes the optimization-based alignment (OBA) method, which is applicable to the in-motion coarse alignment. The OBA algorithm transforms the initial alignment problem into a continuous attitude determination problem by using infinite vector observations. After that, all the constructed vectors during the whole alignment process are used in the initial alignment process to improve the convergence rate. In order to expand the application range of the OBA algorithm, Ref [19] utilizes the devised velocity/position integration formulae to construct the vector observations, and provides the detailed iterative discrete calculation process. Unfortunately, the traditional OBA algorithms mentioned above do not well consider the effects of sensor errors hiding in the vector observation [20]. In order to further improve the accuracy of OBA algorithms, researchers have studied a series of improved OBA algorithms. Ref [21] develops the covariance models for the observation vectors and provides the variance propagation scheme based on error models. Ref [22] utilizes the quaternion estimation (QUEST) algorithm to estimate the initial attitude matrix. The QUEST algorithm constructs *K*-matrix with the

This work is supported by the Natural Science Foundation of Jiangsu Province (BK20221500), the National Natural Science Foundation of China (61703098), and the Fujian Provincial Key Laboratory of Coast and Island Management Technology Study (FJCIMTS2019-03). This work is also supported in part by London Tech Bridge, the APEX Undersea Challenge, the European Regional Development Fund—Industrial Intensive Innovation Programme, the Research Fund from the Science and Technology on Underwater Vehicle Technology Laboratory (2021JCJQ-SYSJJ-LB06905), and the Water Science and Technology Project of Jiangsu Province under grant (2021072, 2021063).

Haoqian Huang, Jiaying Wei and Bing Wang are with College of Energy and Electrical Engineering, Hohai University, Nanjing, China (e-mail: hqhuang@hhu.edu.cn; xtcwjy@hhu.edu.cn; icekingking@hhu.edu.cn).

Di Wang is with the Key Laboratory of Micro-Inertial Instrument and Advanced Navigation Technology, Ministry of Education, School of Instrument Science and Engineering, Southeast University, Nanjing, China, and also with College of Energy and Electrical Engineering, Hohai University, Nanjing, China (e-mail: wangdigood2011@163.com).

Li Zhang is with Department of Computer Science, Royal Holloway, University of London, Surrey, UK (e-mail: li.zhang@rhul.ac.uk).

observation vectors and estimates the optimal attitude quaternion related to *K*-matrix, achieving faster convergence velocity than traditional OBA algorithms. However, this method is limited to the special trajectory of the vehicle. Thus, the REQUEST algorithm is studied in Ref [23], which is based on the QUEST algorithm. The REQUEST algorithm completes recursive processing of observation information by updating *K*-matrix which is utilized in the QUEST algorithm. Although the REQUEST algorithm can suppress the impacts of random noises to some extent, however, it relies on the empirical constant gain to filter measurement noises. This makes the REQUEST algorithm suboptimal and lacks robustness. As an improvement, Ref [24] proposes an Optimal-REQUEST algorithm to determine the attitude quaternion, which can filter the measurement noises by adjusting the gain of the filter adaptively. Nevertheless, the Optimal-REQUEST algorithm is still limited by the scalar gain. The other deficiency is that Optimal-REQUEST algorithm keeps a conservative estimation performance index from REQUEST algorithm. The drawbacks of the Optimal-REQUEST mentioned above limit the accuracy of the in-motion coarse alignment [25]-[26].

In order to improve the performance of the coarse alignment, this paper systematically extends the Optimal-REQUEST algorithm and proposes a new in-motion coarse alignment method. While the AUV is moving on the water, the observation vectors-based measurement model can be constructed by the integration formulae with the assistance of GPS. Then, a Kalman filter based on the vector observation and truncated vectorized *K*-matrix, named the VO-TVK algorithm, is utilized to determine the attitude quaternion. The main contributions of this work are given in the following:

1) The proposed VO-TVK algorithm covers the Optimal-REQUEST algorithm's two deficiencies-using conservative estimation performance index and scalar gain.
2) The random noises contained in the vector observation can be suppressed through the optimal probabilistic fundament of the minimum variance estimation approach. Meanwhile, the VO-TVK algorithm optimally preserves the unit-norm property of the estimated quaternion.
3) The practical experiments have been successfully designed and the feasibility of the VO-TVK algorithm has been verified as being in the practical experiments

The remaining parts of the paper are organized as follows. Section II mathematically formulates the general form of in-motion coarse alignment for SINS/GPS. In Section III, the discrete forms of constructed vectors are derived by considering the different sampling rates of SINS and GPS. Subsequently, the proposed VO-TVK algorithm is developed to implement the in-motion coarse alignment. In Section IV, the efficiency of the VO-TVK algorithm is demonstrated through simulation, vehicle test and lake trial. Finally, the conclusions are outlined in Section V. What is more, Appendix A shows the detailed schematics of the coordinated frames and Appendix B and C represent the detailed formula derivation.

II. SYSTEM DESCRIPTION AND PROBLEM STATEMENT

In this section, the traditional in-motion alignment method is described briefly, and then the existing practical issues are introduced.

A. System Description

According to the chain rule of the attitude matrix, $\mathbf{C}_b^n$ at any time satisfies:

$$\mathbf{C}_b^n(t)=\mathbf{C}_{b(t)}^{n(t)}=\mathbf{C}_{n(0)}^{n(t)}\mathbf{C}_{b(0)}^{n(0)}\mathbf{C}_{b(t)}^{b(0)} \tag{1}$$

where the *n*-frame and *b*-frame represent the navigation frame and body frame, respectively. $\mathbf{C}_{b(t)}^{b(0)}$ and $\mathbf{C}_{n(t)}^{n(0)}$ encode the attitude changes of the body frame and the navigation frame, respectively. Using the attitude update procedure based on $\boldsymbol{\omega}_{ib}^b$ and $\boldsymbol{\omega}_{in}^n$, these two attitude matrices can be determined as follows [13]:

$$\dot{\mathbf{C}}_{b(t)}^{b(0)}=\mathbf{C}_{b(t)}^{b(0)}\boldsymbol{\omega}_{ib}^b\times \tag{2}$$

$$\dot{\mathbf{C}}_{n(t)}^{n(0)}=\mathbf{C}_{n(t)}^{n(0)}\boldsymbol{\omega}_{in}^n\times \tag{3}$$

It is clear that $\mathbf{C}_{b(0)}^{n(0)}$ is always a constant matrix during the alignment. As long as $\mathbf{C}_{b(0)}^{n(0)}$ is obtained accurately, the current attitude matrix $\mathbf{C}_b^n$ can be calculated through Eqs. (1)-(3). According to the basic principle of OBA algorithm, the constant matrix $\mathbf{C}_{b(0)}^{n(0)}$ can be calculated using a series of vector observations which are constructed based on the specific force equation. The specific force equation expression under the navigation frame is given by [15]:

$$\dot{\mathbf{v}}^n=\mathbf{C}_b^n\mathbf{f}^b-(2\boldsymbol{\omega}_{ie}^n+\boldsymbol{\omega}_{en}^n)\times\mathbf{v}^n+\mathbf{g}^n \tag{4}$$

where $\mathbf{v}^n$ and $\mathbf{g}^n$ represent the velocity of the vehicle and the gravity vector in the *n*-frame, respectively; $\mathbf{f}^b$ as the outputs of accelerometers, represents the specific force in the *b*-frame; $\boldsymbol{\omega}_{ie}^n$ denotes the Earth rotation rate with respect to the inertial frame; $\boldsymbol{\omega}_{en}^n$ denotes the angular rate of the navigation frame with respect to the Earth frame.

Combining Eq. (1) and Eq. (4), the following equation can be obtained [19]:

$$\dot{\mathbf{v}}^n=\mathbf{C}_{n(0)}^{n(t)}\mathbf{C}_{b(0)}^{n(0)}\mathbf{C}_{b(t)}^{b(0)}\mathbf{f}^b-(2\boldsymbol{\omega}_{ie}^n+\boldsymbol{\omega}_{en}^n)\times\mathbf{v}^n+\mathbf{g}^n \tag{5}$$

After integration, the original specific force equation can be rewritten into the following form:

$$\mathbf{C}_{b(0)}^{n(0)}\mathbf{C}_{b(t)}^{b(0)}\mathbf{f}^b=\mathbf{C}_{n(t)}^{n(0)}\dot{\mathbf{v}}^n+\mathbf{C}_{n(t)}^{n(0)}(2\boldsymbol{\omega}_{ie}^n+\boldsymbol{\omega}_{en}^n)\times\mathbf{v}^n-\mathbf{C}_{n(t)}^{n(0)}\mathbf{g}^n \tag{6}$$

Next, integrating Eq. (6) and noting that $\mathbf{C}_{b(0)}^{n(0)}$ is constant, the measurement vector and the reference vector can be described as:

$$\mathbf{C}_{b(0)}^{n(0)}\boldsymbol{\alpha}=\boldsymbol{\beta} \tag{7}$$

in which

$$\boldsymbol{\alpha}=\int_0^t\mathbf{C}_{b(\tau)}^{b(0)}\mathbf{f}^b d\tau \tag{8}$$

$$\boldsymbol{\beta}=\mathbf{C}_{n(t)}^{n(0)}\mathbf{v}^n-\mathbf{v}^n(0)+\int_0^t\mathbf{C}_{n(\tau)}^{n(0)}\boldsymbol{\omega}_{ie}^n\times\mathbf{v}^n d\tau-\int_0^t\mathbf{C}_{n(\tau)}^{n(0)}\mathbf{g}^n d\tau \tag{9}$$

Based on the measurement vectors and the reference vectors, the initial attitude $\mathbf{C}_{b(0)}^{n(0)}$ can be determined by the Q-Method. First, the reference vectors and the measurement vectors should

be normalized:

$$\mathbf{r} = \frac{\boldsymbol{\beta}}{\|\boldsymbol{\beta}\|} \tag{10}$$

$$\boldsymbol{\mu} = \frac{\boldsymbol{\alpha}}{\|\boldsymbol{\alpha}\|} \tag{11}$$

Then, use the normalized vectors to calculate the 4 by 4 symmetric *K*-matrix:

$$\mathbf{K}_k = \begin{bmatrix} \mathbf{S}_k - \sigma_k \mathbf{I}_3 & \mathbf{z}_k \\ \mathbf{z}_k^{\mathrm{T}} & \sigma_k \end{bmatrix} \tag{12}$$

where the parameters in Eq. (12) are defined as follows:

$$\mathbf{B}_k \triangleq \sum_{i=1}^{n} a_i \boldsymbol{\mu}_i \mathbf{r}_i^{\mathrm{T}} \tag{13}$$

$$\mathbf{S}_k \triangleq \mathbf{B}_k + \mathbf{B}_k^{\mathrm{T}} \tag{14}$$

$$\mathbf{z}_k \triangleq \sum_{i=1}^{n} a_i \boldsymbol{\mu}_i \times \mathbf{r}_i \tag{15}$$

$$\sigma_k \triangleq tr(\mathbf{B}_k) \tag{16}$$

where $tr(\bullet)$ denotes the trace operator and $\sum_{i=1}^{n} a_i = 1$.

Finally, the corresponding optimal quaternion $\mathbf{q}$ can be calculated by solving the eigenvector of the *K*-matrix corresponding to the largest eigenvalue [27]. The $\mathbf{C}_{b(0)}^{n(0)}$ matrix can be obtained from the optimal quaternion $\mathbf{q}$ to attitude matrix. After that, the attitude angles of vehicles can be acquired by the chain of direction cosine matrix (DCM) using the Eqs. (1)-(3). Unfortunately, the sensors errors and measurement errors of velocity cannot be suppressed well by estimation algorithm with the analytical attitude determination method, which is shown in Eqs. (12)-(16). These formulae are core of the Q-Method, but they only represent analytical models. Therefore, the Q-Method itself does not have the ability to reduce the impact of errors.

B. Problem Statement

According to Section II-A, the general coarse alignment method can be implemented by the measurement vector $\boldsymbol{\mu}$ and reference vector $\mathbf{r}$. As can be observed from Eq. (2) and Eq. (8), $\boldsymbol{\mu}$ is constructed by the true measurements of accelerometers and gyroscopes. However, the outputs of vectors contain the constant biases and the random noises. The noise models are shown as follows:

$$\tilde{\mathbf{f}}^b = \mathbf{f}^b + \nabla^b + \boldsymbol{\eta}_{av} \tag{17}$$

$$\tilde{\boldsymbol{\omega}}_{ib}^b = \boldsymbol{\omega}_{ib}^b + \boldsymbol{\varepsilon}^b + \boldsymbol{\eta}_{gv} \tag{18}$$

where $\tilde{\mathbf{f}}^b = \begin{bmatrix} \tilde{f}_x & \tilde{f}_y & \tilde{f}_z \end{bmatrix}$ denotes the measurement of accelerometers; $\tilde{\boldsymbol{\omega}}_{ib}^b = \begin{bmatrix} \tilde{\omega}_x & \tilde{\omega}_y & \tilde{\omega}_z \end{bmatrix}$ denotes the measurement of gyroscopes; $\mathbf{f}^b$ denotes the true specific force; $\boldsymbol{\omega}_{ib}^b$ denotes the truth angular velocity of the vehicle; ∇^b and $\boldsymbol{\varepsilon}^b$ denote the constant biases of accelerometers and gyroscopes, respectively; $\boldsymbol{\eta}_{av}$ and $\boldsymbol{\eta}_{gv}$ denote the random noises of accelerometers and gyroscopes, respectively.

Assuming that the installation error angles between GPS and SINS have been calibrated in advanced. The scale factor errors are also calibrated before the coarse alignment. Thus, the measurement model of GPS can be modeled as:

$$\tilde{\mathbf{v}}^n = \mathbf{v}^n + \delta\mathbf{v}^n \tag{19}$$

where $\tilde{\mathbf{v}}^n$ represent the measurement of the GPS, $\mathbf{v}^n$ denotes the noise-free velocity, and $\delta\mathbf{v}^n$ is the measurement noise which is assumed to obey Gaussian distribution.

The reference vector $\tilde{\boldsymbol{\beta}}$ can be constructed as:

$$\begin{aligned} \tilde{\boldsymbol{\beta}} &= \mathbf{C}_{n(t)}^{n(0)} \tilde{\mathbf{v}}^n - \tilde{\mathbf{v}}^n(0) + \int_0^t \mathbf{C}_{n(\tau)}^{n(0)} \boldsymbol{\omega}_{ie}^n \times \tilde{\mathbf{v}}^n d\tau - \int_0^t \mathbf{C}_{n(\tau)}^{n(0)} \mathbf{g}^n d\tau \\ &\approx \boldsymbol{\beta} + \mathbf{C}_{n(t)}^{n(0)} \delta\mathbf{v}^n \end{aligned} \tag{20}$$

Because of the short alignment time and small terms, the errors in the first integral on the right are ignored. $\tilde{\mathbf{r}}$ can be acquired by normalized $\tilde{\boldsymbol{\beta}}$.

After that, Eq. (7) can be rewritten as:

$$\mathbf{r} + \mathbf{C}_{n(t)}^{n(0)} \delta\mathbf{v}^n = \mathbf{C}_{b0}^{n0} \boldsymbol{\mu} + \delta\boldsymbol{\Delta} \tag{21}$$

After shifting the item of Eq. (21), the following model can be acquired:

$$\mathbf{r} = \mathbf{C}_{b0}^{n0} \boldsymbol{\mu} + \delta\boldsymbol{\mu} \tag{22}$$

where $\delta\boldsymbol{\mu}$ is additive errors which is composed of the sensors errors and the measurement errors of GPS. Assuming that the sensors errors and the measurement errors of GPS both obey Gaussian distribution, therefore, $\delta\boldsymbol{\mu}$ also obeys Gaussian distribution.

The aforementioned derivation demonstrates that some issues need to be further addressed for the OBA methods. To mitigate the measurement errors that are mixed in the vector observations, a number of efficient approaches have been proposed [28]-[33].

Therefore, inspired by the works mentioned hitherto, this paper proposes an in-motion coarse alignment method based on vector observation and truncated vectorized *K*-matrix. The innovations of the VO-TVK algorithm mainly consist of two aspects, where the VO-TVK algorithm vectorizes the matrix state-space equations of *K*-matrix and truncates the vectorized state vector using the linear dependence between the elements of the *K*-matrix. After that, the minimum variance estimation can be applied to the linear reduced model. Although the measurement noises are considered as Gaussian white noise, it does not impair the generality of the algorithm because there are a few techniques to cope with constant biases in the process noise model. Thus, the proposed VO-TVK algorithm is expected to enhance the accuracy of the traditional OBA algorithm.

III. The Improved In-Motion Coarse Alignment

The above deduction is the general formulation for the coarse alignment of the SINS/GPS integrated navigation system. When the formulae are implemented in the actual system, the sampling rates of SINS and GPS are usually different and the formulae must be discretized before calculation. In this section, the discrete formulae of the vector observation are studied, and the different sampling rates of SINS and GPS are considered.

The VO-TVK algorithm is utilized to update the *K*-matrix and the summarization of the proposed method is given at last.

A. Discrete Formulation of the Vector Observation

To show the different sampling rates of the SINS and GPS, the sampling intervals of SINS and GPS are respectively denoted as Δt_S and Δt_G, namely $\Delta t_G = D\Delta t_S \ \ (D \in N)$. The discrete formulation of the vector observation can be derived as follows.

Firstly, assuming the current alignment time $t = M\Delta t_G$, the first integration of $\boldsymbol{\beta}$ in Eq. (9) can be calculated as [23]:

$$\begin{aligned}
\Delta\mathbf{v}^{n(t_M)} &= \int_0^t \mathbf{C}_{n(\tau)}^{n(0)}\boldsymbol{\omega}_{ie}^n \times \mathbf{v}^n d\tau \\
&= \sum_{k=0}^{M-1}\mathbf{C}_{n(t_k)}^{n(0)}\int_{t_k}^{t_{k+1}}\mathbf{C}_{n(\tau)}^{n(t_k)}\boldsymbol{\omega}_{ie}^n \times \mathbf{v}^n d\tau \\
&\approx \sum_{k=0}^{M-1}\mathbf{C}_{n(t_k)}^{n(0)}\int_{t_k}^{t_{k+1}}\left[\mathbf{I}+(\tau-t_k)\boldsymbol{\omega}_{in}^n\times\right]\boldsymbol{\omega}_{ie}^n \times \\
&\quad \left[\mathbf{v}^n(t_k)+\frac{\tau-t_k}{\Delta t_G}\left(\mathbf{v}^n(t_{k+1})-\mathbf{v}^n(t_k)\right)\right]d\tau \\
&= \sum_{k=0}^{M-1}\mathbf{C}_{n(t_k)}^{n(0)}\left[\left(\Delta t_G\mathbf{I}+\frac{\Delta t_G^2}{2}\boldsymbol{\omega}_{in}^n\times\right)\boldsymbol{\omega}_{ie}^n\times\mathbf{v}^n(t_k)+\right. \\
&\quad \left.\left(\frac{\Delta t_G}{2}\mathbf{I}+\frac{\Delta t_G^2}{3}\boldsymbol{\omega}_{in}^n\times\right)\boldsymbol{\omega}_{ie}^n\times\left(\mathbf{v}^n(t_{k+1})-\mathbf{v}^n(t_k)\right)\right] \\
&= \sum_{k=0}^{M-1}\mathbf{C}_{n(t_k)}^{n(0)}\left[\left(\frac{\Delta t_G}{2}\mathbf{I}+\frac{\Delta t_G^2}{6}\boldsymbol{\omega}_{in}^n\times\right)\boldsymbol{\omega}_{ie}^n\times\mathbf{v}^n(t_k)+\right. \\
&\quad \left.\left(\frac{\Delta t_G}{2}\mathbf{I}+\frac{\Delta t_G^2}{3}\boldsymbol{\omega}_{in}^n\times\right)\boldsymbol{\omega}_{ie}^n\times\mathbf{v}^n(t_{k+1})\right]
\end{aligned} \tag{23}$$

The second integration of $\boldsymbol{\beta}$ in Eq. (9) can be calculated as:

$$\begin{aligned}
\int_0^t \mathbf{C}_{n(\tau)}^{n(0)}\mathbf{g}^n d\tau &\approx \sum_{k=0}^{M-1}\mathbf{C}_{n(t_k)}^{n(0)}\int_{t_k}^{t_{k+1}}\mathbf{C}_{n(\tau)}^{n(t_k)}\mathbf{g}^n d\tau \\
&= \sum_{k=0}^{M-1}\mathbf{C}_{n(t_k)}^{n(0)}\int_{t_k}^{t_{k+1}}\left[\mathbf{I}+(\tau-t_k)\boldsymbol{\omega}_{in}^n\times\right]\mathbf{g}^n d\tau \\
&= \sum_{k=0}^{M-1}\mathbf{C}_{n(t_k)}^{n(0)}\left(\Delta t_G\mathbf{I}+\frac{\Delta t_G^2}{2}\boldsymbol{\omega}_{in}^n\times\right)\mathbf{g}^n
\end{aligned} \tag{24}$$

Secondly, the integration of $\boldsymbol{\alpha}$ in Eq. (8) can be calculated similar to the first assumption:

$$\boldsymbol{\alpha} = \int_0^t \mathbf{C}_{b(\tau)}^{b(0)}\mathbf{f}^b d\tau = \sum_{k=0}^{M-1}\mathbf{C}_{b(t_k)}^{b(0)}\int_{t_k}^{t_{k+1}}\mathbf{C}_{b(\tau)}^{b(t_k)}\mathbf{f}^b d\tau \tag{25}$$

The incremental integral in Eq. (25) can be approximated using the two-sample method. The specific calculation is as follows**:**

$$\begin{aligned}
\Delta\mathbf{v}^{b(t_M)} &= \int_{t_k}^{t_{k+1}}\mathbf{C}_{b(\tau)}^{b(t_k)}\mathbf{f}^b d\tau = \int_{t_k}^{t_{k+1}}\left[\mathbf{I}+(\int_{t_k}^{t}\omega_{ib}^b d\tau)\times\right]\mathbf{f}^b d\tau \\
&= \Delta\mathbf{v}_1+\Delta\mathbf{v}_2+\frac{1}{2}(\Delta\boldsymbol{\theta}_1+\Delta\boldsymbol{\theta}_2)\times(\Delta\mathbf{v}_1+\Delta\mathbf{v}_2)+ \\
&\quad \frac{2}{3}(\Delta\boldsymbol{\theta}_1\times\Delta\mathbf{v}_2+\Delta\mathbf{v}_1\times\Delta\boldsymbol{\theta}_2)
\end{aligned} \tag{26}$$

where

$$\Delta\mathbf{v}_1 = \sum_{l=1}^{\frac{D}{2}}\mathbf{f}_{k,l}^b\Delta t_S, \quad \Delta\mathbf{v}_2 = \sum_{l=\frac{D}{2}+1}^{D}\mathbf{f}_{k,l}^b\Delta t_S \tag{27}$$

$$\Delta\boldsymbol{\theta}_1 = \sum_{l=1}^{\frac{D}{2}}\boldsymbol{\omega}_{ib,k,l}^b\Delta t_S, \quad \Delta\boldsymbol{\theta}_2 = \sum_{l=\frac{D}{2}+1}^{D}\boldsymbol{\omega}_{ib,k,l}^b\Delta t_S \tag{28}$$

Using Eqs. (2)-(3), the DCM $\mathbf{C}_{n(t_{k+1})}^{n(t_k)}$ and $\mathbf{C}_{b(t_{k+1})}^{b(t_k)}$ can be calculated [23]:

$$\mathbf{C}_{n(t_{k+1})}^{n(t_k)} = \mathbf{I}+\frac{\sin\left\|\Theta_{in}^n\right\|}{\left\|\Theta_{in}^n\right\|}[\Theta_{in}^n\times]+\frac{1-\cos\left\|\Theta_{in}^n\right\|}{\left\|\Theta_{in}^n\right\|^2}[\Theta_{in}^n\times]^2 \tag{29}$$

$$\mathbf{C}_{b(t_{k+1})}^{b(t_k)} = \mathbf{I}+\frac{\sin\left\|\Theta_{ib}^b\right\|}{\left\|\Theta_{ib}^b\right\|}[\Theta_{ib}^b\times]+\frac{1-\cos\left\|\Theta_{ib}^b\right\|}{\left\|\Theta_{ib}^b\right\|^2}[\Theta_{ib}^b\times]^2 \tag{30}$$

where

$$\begin{cases}
\Theta_{in}^n \approx \boldsymbol{\omega}_{in}^n\Delta t_G \\
\Theta_{ib}^b = \sum_{l=1}^{D}\boldsymbol{\omega}_{ib,l}^b\Delta t_S
\end{cases} \tag{31}$$

where $\Delta t_G = t_{k+1}-t_k$; $\boldsymbol{\omega}_{ib,l}^b$ denotes the *l*th angular rate of the gyroscope measurement during t_k to t_{k+1}; $\boldsymbol{\omega}_{in}^n = \boldsymbol{\omega}_{ie}^n+\boldsymbol{\omega}_{en}^n$ is the angular rate of *n*-frame with respect to the *i*-frame. Due to the short alignment time and relatively slow speed of the vehicle, the rotating rate $\boldsymbol{\omega}_{in}^n$ is approximate to $\boldsymbol{\omega}_{ie}^n$. Moreover, $\boldsymbol{\omega}_{ie}^n$ can be acquired easily by the position of inertial measurement unit (IMU) and the Earth rotation rate.

Finally, using Eqs. (9), (23) and (24), the discrete form of the vector $\boldsymbol{\beta}$ can be written as:

$$\boldsymbol{\beta}_M = \mathbf{C}_{n(t_M)}^{n(0)}\mathbf{v}_M^n-\mathbf{v}^n(0)+\Delta\mathbf{v}^{n(t_M)}-\sum_{k=0}^{M-1}\mathbf{C}_{n(t_k)}^{n(0)}\left(\Delta t_G\mathbf{I}+\Delta t_G^2\frac{\boldsymbol{\omega}_{in}^n\times}{2}\right)\mathbf{g}^n \tag{32}$$

Using Eqs. (25)-(28), the discrete form of the vector $\boldsymbol{\alpha}$ can be written as:

$$\begin{aligned}
\boldsymbol{\alpha}_M &= \boldsymbol{\alpha}_{M-1}+\mathbf{C}_{b(M-1)}^{b0}\left[\Delta\mathbf{v}_1+\Delta\mathbf{v}_2+\frac{1}{2}(\Delta\boldsymbol{\theta}_1+\Delta\boldsymbol{\theta}_2)\times(\Delta\mathbf{v}_1+\Delta\mathbf{v}_2)\right. \\
&\quad \left.+\frac{2}{3}(\Delta\boldsymbol{\theta}_1\times\Delta\mathbf{v}_2+\Delta\mathbf{v}_1\times\Delta\boldsymbol{\theta}_2)\right]
\end{aligned} \tag{33}$$

With Eqs. (29)-(31), the initial DCM can be determined by the OBA algorithm. However, the OBA algorithm does not well mitigate the errors which come from the inertial sensors' and GPS's measurements. In the next subsection, a Kalman filter based on the truncated vectorized *K*-matrix is designed to circumvent the defects of the traditional OBA algorithms.

B. Filtering Design

The construction of the time-varying *K*-matrix is shown in Eqs. (10)-(16). Before filtering, the process model and measurement model of *K*-matrix must be deducted.

1) Process equation: The propagation of the *K*-matrix from t_k to t_{k+1} yields $\mathbf{K}_{k+1}$, defined below:

$$\mathbf{K}_{k+1} = \boldsymbol{\Phi}_k\mathbf{K}_k\boldsymbol{\Phi}_k^{\mathrm{T}} \tag{34}$$

where t_k and t_{k+1} represent the time of *k* and *k*+1 moment. $\boldsymbol{\Phi}_k$ is the transition matrix in the difference equation that governs the following discrete-time dynamics of the quaternion.

$$\mathbf{q}_{k+1} = \boldsymbol{\Phi}_k\mathbf{q}_k \tag{35}$$

During the coarse alignment, the quaternion corresponding to the *K*-matrix is always at the initial moment, thus $\mathbf{\Phi}_k = \mathbf{I}_4$.

Taking the symmetry and zero-trace of the *K*-matrix into account, the number of independent elements can be reduced to nine. See Appendix C for the proof of the *K*-matrix's zero-trace characteristic. After truncating the *K*-matrix, the state variable is constructed as:

$$\mathbf{x}_k \triangleq \begin{bmatrix} K_{k_{11}} & K_{k_{12}} & K_{k_{13}} & K_{k_{14}} & K_{k_{22}} & K_{k_{23}} & K_{k_{24}} & K_{k_{33}} & K_{k_{34}} \end{bmatrix}^{\mathrm{T}} \quad (36)$$

where $K_{k_{i,j}}$ denotes the element of $\mathbf{K}_k$ at position (i, j).

Then, the process model of the *K*-matrix can be written as:

$$\mathbf{x}_{k+1} = \mathbf{\Psi}_k \mathbf{x}_k \quad (37)$$

where $\mathbf{x}_{k+1}$ is the 9×1 state vector at the time of t_{k+1}; $\mathbf{\Psi}_k = \mathbf{I}_9$.

2) Measurement equation: When a batch of independent observations $\boldsymbol{\mu}_{k+1}^i$ and $\mathbf{r}_{k+1}^i$ are observed simultaneously ($i = 1, 2, \cdots, n$) at the time of t_{k+1}, the corresponding incremental *K*-matrix $\delta\mathbf{K}_{k+1}$ can be calculated as:

$$\delta\mathbf{K}_{k+1} = \begin{bmatrix} \mathbf{S}_{k+1} - \sigma_{k+1}\mathbf{I}_3 & \mathbf{z}_{k+1} \\ \mathbf{z}_{k+1}^{\mathrm{T}} & \sigma_{k+1} \end{bmatrix} \quad (38)$$

where the parameters in Eq. (38) are defined as:

$$\mathbf{B}_{k+1} \triangleq \sum_{i=1}^{n} a_i \boldsymbol{\mu}_i \mathbf{r}_i^{\mathrm{T}} \quad (39)$$

$$\mathbf{S}_{k+1} \triangleq \mathbf{B}_{k+1} + \mathbf{B}_{k+1}^{\mathrm{T}} \quad (40)$$

$$\mathbf{z}_{k+1} \triangleq \sum_{i=1}^{n} a_i \boldsymbol{\mu}_i \times \mathbf{r}_i \quad (41)$$

$$\sigma_{k+1} \triangleq tr(\mathbf{B}_{k+1}) \quad (42)$$

Considering that $\delta\mathbf{K}_{k+1}$ is calculated using the noisy measurements acquired at the time of t_{k+1}, the *K*-matrix measurement model can be described as:

$$\delta\mathbf{K}_{k+1} = \mathbf{K}_{k+1} + \mathbf{V}_{k+1} \quad (43)$$

The measurement noise matrix $\mathbf{V}_{k+1}$ is shown as:

$$\mathbf{V}_{k+1} = \begin{bmatrix} \mathbf{S}_\mu - \sigma_\mu \mathbf{I}_3 & \mathbf{z}_\mu \\ \mathbf{z}_\mu^{\mathrm{T}} & \sigma_\mu \end{bmatrix} \quad (44)$$

where the parameters in Eq. (44) are defined as:

$$\mathbf{B}_\mu \triangleq \sum_{i=1}^{n} a_i \delta\boldsymbol{\mu}_{k+1}^i (\mathbf{r}_{k+1}^i)^{\mathrm{T}} \quad (45)$$

$$\mathbf{S}_\mu \triangleq \mathbf{B}_\mu + \mathbf{B}_\mu^{\mathrm{T}} \quad (46)$$

$$\mathbf{z}_\mu \triangleq \sum_{i=1}^{n} a_i \delta\boldsymbol{\mu}_{k+1}^i \times \mathbf{r}_{k+1}^i \quad (47)$$

$$\sigma_\mu \triangleq tr(\mathbf{B}_\mu) \quad (48)$$

where $\delta\boldsymbol{\mu}_{k+1}^i$ denotes the random noises of the measurement results in measurement vector at t_{k+1}. Similarly to $\mathbf{x}_k$, the vectors $\mathbf{x}_{k+1}$ and $\mathbf{y}_{k+1}$ can be defined using the elements of the matrices $\mathbf{K}_{k+1}$ and $\delta\mathbf{K}_{k+1}$. When a batch of independent observations $\boldsymbol{\mu}_{k+1}^i$ and $\mathbf{r}_{k+1}^i$ are observed simultaneously, $i = 1, 2, \cdots, n$, the measurement equation can be presented as follows:

$$\mathbf{y}_{k+1} = \mathbf{x}_{k+1} + \mathbf{v}_{k+1}^n \quad (49)$$

$$\mathbf{v}_{k+1}^n = \sum_{i=1}^{n} a_i \mathbf{\Lambda}_{k+1}^i \delta\boldsymbol{\mu}_{k+1}^i \quad (50)$$

where a_i represents the weight associated with the i^{th} vector measurement at t_{k+1}, which $\sum_{i=1}^{n} a_i = 1$; $\mathbf{\Lambda}_{k+1}^i$ is defined as:

$$\mathbf{\Lambda}_{k+1}^i \triangleq \begin{bmatrix} r_{k+1_1}^i & -r_{k+1_2}^i & -r_{k+1_3}^i \\ r_{k+1_2}^i & r_{k+1_1}^i & 0 \\ r_{k+1_3}^i & 0 & r_{k+1_1}^i \\ 0 & r_{k+1_3}^i & -r_{k+1_2}^i \\ -r_{k+1_1}^i & r_{k+1_2}^i & -r_{k+1_3}^i \\ 0 & r_{k+1_3}^i & r_{k+1_2}^i \\ -r_{k+1_3}^i & 0 & r_{k+1_1}^i \\ -r_{k+1_1}^i & -r_{k+1_2}^i & r_{k+1_3}^i \\ r_{k+1_2}^i & -r_{k+1_1}^i & 0 \end{bmatrix} \quad (51)$$

where the scalars $r_{k+1_1}^i$, $r_{k+1_2}^i$, $r_{k+1_3}^i$ denote the three components of the vector $\mathbf{r}_{k+1}^i$.

Proof: See Appendix B.

3) Noise stochastic models: The error in the i^{th} vector measurement at the time of t_{k+1} is modelled as a zero-mean white noise with a known covariance matrix $\mathbf{R}_{k+1}^i$:

$$E\left[\delta\boldsymbol{\mu}_{k+1}^i \quad (\delta\boldsymbol{\mu}_{k+1}^i)^{\mathrm{T}}\right] = \mathbf{R}_{k+1}^i \quad (52)$$

Furthermore, it is assumed that the measurement vectors calculated at the time of *k*+1 are uncorrelated. When $i \neq j$, the following equation holds:

$$E\left[\delta\boldsymbol{\mu}_{k+1}^i \quad (\delta\boldsymbol{\mu}_{k+1}^j)^{\mathrm{T}}\right] = \mathbf{0}_3 \quad (53)$$

where $\mathbf{0}_3$ is the 3×3 null matrix. After assuming that $\boldsymbol{\delta\mu}_{k+1}^i$ is uncorrelated with $\mathbf{x}_0$, the expectation matrix of the measurement noise $\mathbf{v}_{k+1}^n$ is calculated as:

$$E\left[\mathbf{v}_{k+1}^n\right] = E\left[\sum_{i=1}^{n} a_i \Lambda_{k+1}^i \delta\boldsymbol{\mu}_{k+1}^i\right] = \sum_{i=1}^{n} a_i \Lambda_{k+1}^i E\left[\delta\boldsymbol{\mu}_{k+1}^i\right] = \mathbf{0} \quad (54)$$

The covariance matrix $\mathbf{R}_{k+1}$ is given as:

$$\begin{aligned} \mathbf{R}_{k+1} &\triangleq E\left[\mathbf{v}_{k+1}^n (\mathbf{v}_{k+1}^n)^{\mathrm{T}}\right] = E\left[\sum_{i=1}^{n}\sum_{j=1}^{n} a_i a_j \mathbf{\Lambda}_{k+1}^i \boldsymbol{\delta\mu}_{k+1}^i (\boldsymbol{\delta\mu}_{k+1}^j)^{\mathrm{T}} (\mathbf{\Lambda}_{k+1}^j)^{\mathrm{T}}\right] \\ &= \sum_{i=1}^{n}\sum_{j=1}^{n} a_i a_j \mathbf{\Lambda}_{k+1}^i E\left[\boldsymbol{\delta\mu}_{k+1}^i (\boldsymbol{\delta\mu}_{k+1}^j)^{\mathrm{T}}\right] (\mathbf{\Lambda}_{k+1}^j)^{\mathrm{T}} \\ &= \sum_{i=1}^{n}\sum_{j=1}^{n} a_i a_j \mathbf{\Lambda}_{k+1}^i \delta_{ij} \mathbf{R}_{k+1}^i (\mathbf{\Lambda}_{k+1}^j)^{\mathrm{T}} = \sum_{i=1}^{n} a_i^2 \mathbf{\Lambda}_{k+1}^i \mathbf{R}_{k+1}^i (\mathbf{\Lambda}_{k+1}^i)^{\mathrm{T}} \end{aligned} \quad (55)$$

where δ_{ij} is the Kronecker delta.

4) Kalman filter summary: A linear Kalman filter is applied to the 9×9 linear model which is described in Eq. (37) and Eqs.

(49)-(50). To distinguish the Kalman gain and *K*-matrix, the Kalman gain here is denoted by $\mathbf{G}_{k+1}$.

Step 1 Initialization:

$$\hat{\mathbf{x}}_{0/0} = \mathbf{y}_0 \tag{56}$$

Step 2 Time Update:

$$\hat{\mathbf{x}}_{k+1/k} = \boldsymbol{\Psi}_k \hat{\mathbf{x}}_{k/k} \tag{57}$$

$$\mathbf{P}_{k+1/k} = \boldsymbol{\Psi}_k \mathbf{P}_{k/k} \boldsymbol{\Psi}_k^{\mathrm{T}} \tag{58}$$

where $\boldsymbol{\Psi}_k = \mathbf{I}_9$.

Step 3 Measurement Update:

$$\mathbf{G}_{k+1} = \mathbf{P}_{k+1/k}(\mathbf{P}_{k+1/k} + \mathbf{R}_{k+1})^{-1} \tag{59}$$

$$\hat{\mathbf{x}}_{k+1/k+1} = \hat{\mathbf{x}}_{k+1/k} + \mathbf{G}_{k+1}(\mathbf{y}_{k+1} - \hat{\mathbf{x}}_{k+1/k}) \tag{60}$$

$$\mathbf{P}_{k+1/k+1} = (\mathbf{I}_9 - \mathbf{G}_{k+1})\mathbf{P}_{k+1/k}(\mathbf{I}_9 - \mathbf{G}_{k+1})^{\mathrm{T}} + \mathbf{G}_{k+1}\mathbf{R}_{k+1}\mathbf{G}_{k+1}^{\mathrm{T}} \tag{61}$$

$$\mathbf{R}_{k+1} \triangleq E\left[\mathbf{v}_{k+1}^n (\mathbf{v}_{k+1}^n)^{\mathrm{T}}\right] = \sum_{i=1}^{n} a_i \boldsymbol{\Lambda}_{k+1}^i \mathbf{R}_{k+1}^i (\boldsymbol{\Lambda}_{k+1}^i)^{\mathrm{T}} \tag{62}$$

where $\boldsymbol{\Lambda}_{k+1}^i$ is calculated using Eq. (51).

5) Quaternion computation: Utilizing the updated estimated of the state vector $\hat{\mathbf{x}}$, the variable $\hat{\boldsymbol{x}}_{10}$ can be calculated:

$$\hat{x}_{10} = -(\hat{x}_1 + \hat{x}_5 + \hat{x}_8) \tag{63}$$

Then, the updated matrix $\hat{\mathbf{K}}$ can be reconstructed:

$$\hat{\mathbf{K}} = \begin{bmatrix} \hat{x}_1 & \hat{x}_2 & \hat{x}_3 & \hat{x}_4 \\ \hat{x}_2 & \hat{x}_5 & \hat{x}_6 & \hat{x}_7 \\ \hat{x}_3 & \hat{x}_6 & \hat{x}_8 & \hat{x}_9 \\ \hat{x}_4 & \hat{x}_7 & \hat{x}_9 & \hat{x}_{10} \end{bmatrix} \tag{64}$$

Finally, the eigenvector corresponding to the maximum eigenvalue of *K*-matrix is calculated, and the optimal quaternion is converted into an attitude matrix to complete the in-motion coarse alignment process.

C. Algorithm Description

Fig. 1 summarizes the in-motion coarse alignment procedure of the proposed TVK algorithm, and the specific algorithm procedure is shown in Table I.

TABLE I

THE PROPOSED VO-TVK ALGORITHM

Initialization: $M = 1$, $\mathbf{C}_{b(0)}^{b0} = \mathbf{C}_{n(0)}^{n0} = \mathbf{I}_3$, $\boldsymbol{\alpha}_0 = \boldsymbol{\beta}_0 = \mathbf{0}$

Inputs: $\left\{\mathbf{f}^b\right\}_{k=1}^{M}, \left\{\boldsymbol{\omega}_{ib}^b\right\}_{k=1}^{M}, \left\{\mathbf{v}^n\right\}_{k=1}^{M}, \{L\}_{k=1}^{M}$

Outputs:

$\mathbf{C}_b^n$: the initial attitude matrix of vehicles.

for ***k*****=1, 2, 3, …, *n*, do**

%Construct the observation vectors:

Calculate $\mathbf{C}_{n(t_k)}^{n(0)}$ and $\mathbf{C}_{b(t_k)}^{b(0)}$ using $\boldsymbol{\omega}_{in}^n$ and $\boldsymbol{\omega}_{ib}^b$ by:

$$\mathbf{C}_{n(t_k)}^{n(0)} = \mathbf{C}_{n(t_{k-1})}^{n(0)} \left(\mathbf{I} + \frac{\sin\left\|\Theta_{in}^n\right\|}{\left\|\Theta_{in}^n\right\|}[\Theta_{in}^n\times] + \frac{1-\cos\left\|\Theta_{in}^n\right\|}{\left\|\Theta_{in}^n\right\|^2}[\Theta_{in}^n\times]^2 \right)$$

$$\mathbf{C}_{b(t_k)}^{b(0)} = \mathbf{C}_{b(t_{k-1})}^{b(0)} \left(\mathbf{I} + \frac{\sin\left\|\Theta_{ib}^b\right\|}{\left\|\Theta_{ib}^b\right\|}[\Theta_{ib}^b\times] + \frac{1-\cos\left\|\Theta_{ib}^b\right\|}{\left\|\Theta_{ib}^b\right\|^2}[\Theta_{ib}^b\times]^2 \right)$$

Calculate $\Delta\mathbf{v}_1$, $\Delta\mathbf{v}_2$, $\Delta\boldsymbol{\theta}_1$ and $\Delta\boldsymbol{\theta}_2$ by the two-sample method.

if GPS outputs are available

Calculate the measurement vectors:

$$\boldsymbol{\beta}'_M = \boldsymbol{\beta}'_{M-1} + \mathbf{C}_{n(t_{M-1})}^{n(0)} \left[\left(\frac{\Delta t_G}{2}\mathbf{I} + \frac{\Delta t_G^2}{6}\boldsymbol{\omega}_{in}^n\times \right)\boldsymbol{\omega}_{ie}^n\times\mathbf{v}^n(t_{M-1}) + \left(\frac{\Delta t_G}{2}\mathbf{I} + \frac{\Delta t_G^2}{3}\boldsymbol{\omega}_{in}^n\times \right)\boldsymbol{\omega}_{ie}^n\times\mathbf{v}^n(t_M) - \left(\Delta t_G\mathbf{I} + \frac{\Delta t_G^2}{2}\boldsymbol{\omega}_{in}^n\times \right)\mathbf{g}^n \right]$$

$$\boldsymbol{\beta}_M = \mathbf{C}_{n(t_M)}^{n(0)}\mathbf{v}_M^n - \mathbf{v}^n(0) + \boldsymbol{\beta}'_M$$

Calculate the reference vectors:

$$\boldsymbol{\alpha}_M = \boldsymbol{\alpha}_{M-1} + \mathbf{C}_{b(t_{M-1})}^{b(0)} \left[\Delta\mathbf{v}_1 + \Delta\mathbf{v}_2 + \frac{1}{2}(\Delta\boldsymbol{\theta}_1 + \Delta\boldsymbol{\theta}_2)\times(\Delta\mathbf{v}_1 + \Delta\mathbf{v}_2) + \frac{2}{3}(\Delta\boldsymbol{\theta}_1\times\Delta\mathbf{v}_2 + \Delta\mathbf{v}_1\times\Delta\boldsymbol{\theta}_2) \right]$$

%Calculate *K*-matrix:

if $M = 1$

The $\mathbf{K}_1$ matrix can be constructed by Eqs. (12)-(16).

$\mathbf{x}_0$ can be calculated by the truncated vectorized $\mathbf{K}_1$ matrix as follows:

$$\mathbf{x}_0 \triangleq \left[K_{1_{11}} \quad K_{1_{12}} \quad K_{1_{13}} \quad K_{1_{14}} \quad K_{1_{22}} \quad K_{1_{23}} \quad K_{1_{24}} \quad K_{1_{33}} \quad K_{1_{34}} \right]^{\mathrm{T}}$$

Initialize Kalman filter by:

$\mathbf{x}_0 = \mathbf{y}_0$

else if

The $\delta\mathbf{K}_M$ matrix can be constructed by Eqs. (38)-(42).

$\mathbf{y}_{t_k}$ can be calculated by the truncated vectorized $\delta\mathbf{K}_M$ matrix:

$$\mathbf{y}_{t_k} \triangleq \left[\delta K_{t_{k_{11}}} \quad \delta K_{t_{k_{12}}} \quad \delta K_{t_{k_{13}}} \quad \delta K_{t_{k_{14}}} \quad \delta K_{t_{k_{22}}} \quad \delta K_{t_{k_{23}}} \quad \delta K_{t_{k_{24}}} \quad \delta K_{t_{k_{33}}} \quad \delta K_{t_{k_{34}}} \right]^{\mathrm{T}}$$

end if

%Update *K*-matrix:

Update time by:

$$\hat{\mathbf{x}}_{k+1/k} = \boldsymbol{\Psi}_k \hat{\mathbf{x}}_{k/k}$$

$$\mathbf{P}_{k+1/k} = \boldsymbol{\Psi}_k \mathbf{P}_{k/k} \boldsymbol{\Psi}_k^{\mathrm{T}}$$

Update measurement by the following equations and Eq. (51):

$$\mathbf{G}_{k+1} = \mathbf{P}_{k+1/k}(\mathbf{P}_{k+1/k} + \mathbf{R}_{k+1})^{-1}$$

$$\hat{\mathbf{x}}_{k+1/k+1} = \hat{\mathbf{x}}_{k+1/k} + \mathbf{G}_{k+1}(\mathbf{y}_{k+1} - \hat{\mathbf{x}}_{k+1/k})$$

$$\mathbf{P}_{k+1/k+1} = (\mathbf{I}_9 - \mathbf{G}_{k+1})\mathbf{P}_{k+1/k}(\mathbf{I}_9 - \mathbf{G}_{k+1})^{\mathrm{T}} + \mathbf{G}_{k+1}\mathbf{R}_{k+1}\mathbf{G}_{k+1}^{\mathrm{T}}$$

$$\mathbf{R}_{k+1} \triangleq E\left[\mathbf{v}_{k+1}^n (\mathbf{v}_{k+1}^n)^{\mathrm{T}}\right] = \sum_{i=1}^{n} a_i \boldsymbol{\Lambda}_{k+1}^i \mathbf{R}_{k+1}^i (\boldsymbol{\Lambda}_{k+1}^i)^{\mathrm{T}}$$

Reconstruct the updated $\hat{\mathbf{K}}_M$ by Eqs. (63)-(64).

Calculate the maximum eigenvector of $\hat{\mathbf{K}}_M$.

Extract $\mathbf{q}_{n0}^{b0}$ from $\hat{\mathbf{K}}_M$ and transform to $\mathbf{C}_{n0}^{b0}$

$M = M + 1$

end if

Calculate the current attitude according to:

$$\mathbf{C}_b^n(t_k) = \mathbf{C}_{n(0)}^{n(t_k)}\mathbf{C}_{n(0)}^{n(0)}\mathbf{C}_{b(0)}^{b(0)}\mathbf{C}_{b(t_k)}^{b(0)}$$

end for

IV. PERFORMANCE EVALUATION

In this section, the simulation, vehicle test and lake trial are designed to verify the performance of the VO-TVK algorithm.

A. Simulation Test

In this simulation test, the well-defined trajectory is set in advance, and the actual information of the vehicle's movement is known. Thus, the actual angles can be used as reference information to evaluate the performance of the proposed VO-TVK method.

The motion process of vehicle is listed in Table II , where the different motion modes are simulated including uniform, acceleration, turning. Figs. 2-4 show the zigzag trajectory and the reference information (angles and velocity) of the vehicle. The output frequencies of the simulated inertial measurement units and GPS are set as 100Hz and 1Hz. Meanwhile, the constant biases and random noises of three-axis gyroscope,

three-axis accelerometer and GPS are given in Table III. The initial position of the vehicle is set as L=32.00° and λ=118.00°, where L denotes the latitude, and λ denotes the longitude.

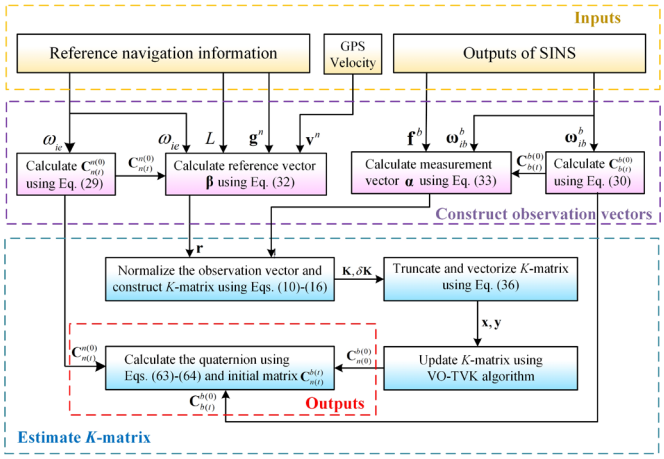

Fig. 1. The in-motion initial alignment procedure using the proposed VO-TVK algorithm.

TABLE II

PROCESS OF THE VEHICLE MOTION IN THE SIMULATION TEST

Number	Movement State	Time(s)
1	Accelerated ($a=0.5m/s^2$)	0~20s
2	Uniform	20~40s
3	Turn right ($\omega_z=4rad/s$)	40~60s
4	Uniform	60~160s
5	Turn left ($\omega_z=-4rad/s$)	160~180s
6	Uniform	180~250s

TABLE III

CONSTANT BIAS AND RANDOM NOISE OF THE SENSORS IN THE SIMULATION

Sensors	Constant biases	Random noise
Gyroscopes	0.01 deg/h	0.01 deg/$\sqrt{\text{h}}$
Accelerometers	10 ug	100 ug /$\sqrt{\text{Hz}}$
GPS	0 m/s	1 m/s

During the whole initial alignment, the vehicle is moving on the horizontal plane and the total simulation time is 250s. To improve the credibility of simulation, the initial value of pitch, roll and yaw angles are respectively set as 3°, 3° and 10°. Besides, we choose the Q-Method algorithm, the REQUEST algorithm, the Optimal-REQUEST algorithm and the proposed VO-TVK algorithm to tested and compared. Figs. 5-7 are the alignment errors of the pitch, roll and yaw angles, respectively.

In Fig. 5, it can be found that four algorithms have similar convergence rates. However, the other three algorithms except VO-TVK all fluctuate when the significant changes have taken place on roll angle. The proposed VO-TVK is the most stable and the accuracy is also improved with the increase of alignment time.

As seen from Fig. 6, the stability of the proposed VO-TVK algorithm can be better proved in the calculation of roll angles. When the vehicle has turning action, the other three comparison algorithms all have large fluctuations. However, the proposed VO-TVK algorithm has not been affected, remaining stable and precise.

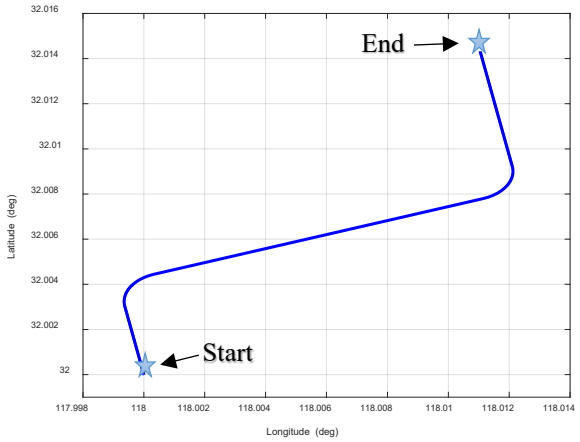

Fig. 2. Trajectory of the vehicle in the simulation test.

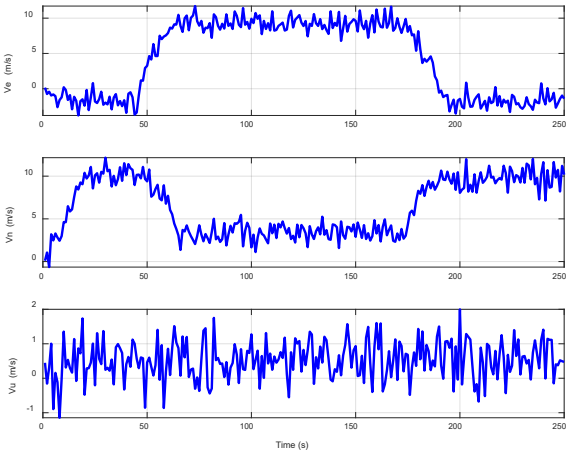

Fig. 3. Reference velocity in the simulation test.

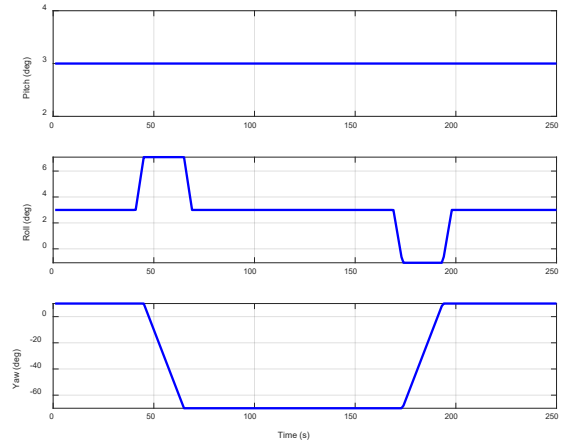

Fig. 4. Reference attitude in the simulation test.

Fig. 7 gives the yaw errors of four algorithms, and it can illustrate the advantages of the proposed VO-TVK algorithm well. To verify the performances of the VO-TVK algorithm and compared algorithms, the errors of velocity are set obviously. It is known that the velocity of GPS has a great influence on the

This article has been accepted for publication in IEEE Transactions on Instrumentation and Measurement. This is the author's version which has not been fully edited and content may change prior to final publication. Citation information: DOI 10.1109/TIM.2022.3196431

calculation of yaw angle. The Q-Method algorithm does not have the ability to alleviate the impact of errors hiding in the vector observation which results in the unsatisfactory alignment results. Meanwhile, the REQUEST algorithm utilizes the empirical constant gain to update the *K*-matrix and it is hard to find the appropriate value because the errors are cumulative during the alignment process. Thus, the accuracy of Q-Method and REQUEST algorithm are both poor in Fig. 7. What is more, the Optimal-REQUEST algorithm is hard to be performed well in the simulation test due to the conservative estimation performance index. The proposed VO-TVK algorithm combines the advantages of the Wahba problem and the Kalman filtering. It can well alleviate the influence of vector observation errors on alignment results. Meanwhile, it gets rid of the limits of empirical constant gain and conservative estimation performance index. Thus, the VO-TVK overcomes the impact of errors and maintains stability. Considering the alignment results of three angles, we find that the VO-TVK algorithm is the most stable and most precise alignment approach compared with the Q-Method, the REQUEST and the Optimal-REQUEST algorithm.

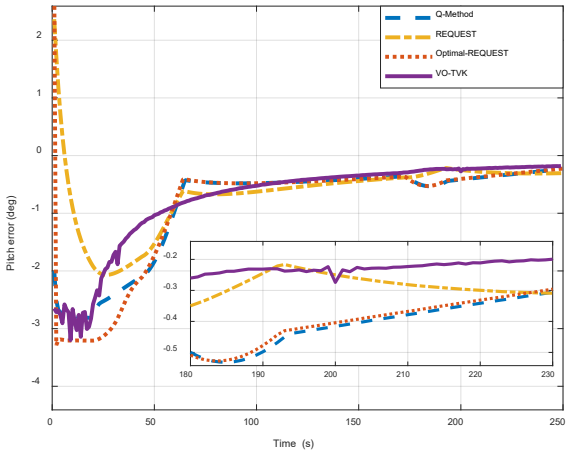

Fig. 5. Curves of pitch angle errors.

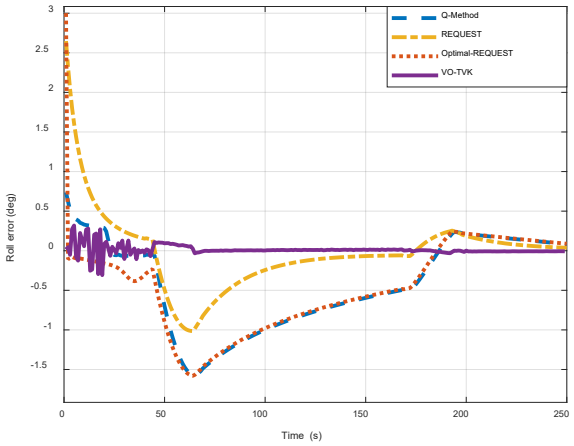

Fig. 6. Curves of roll angle errors.

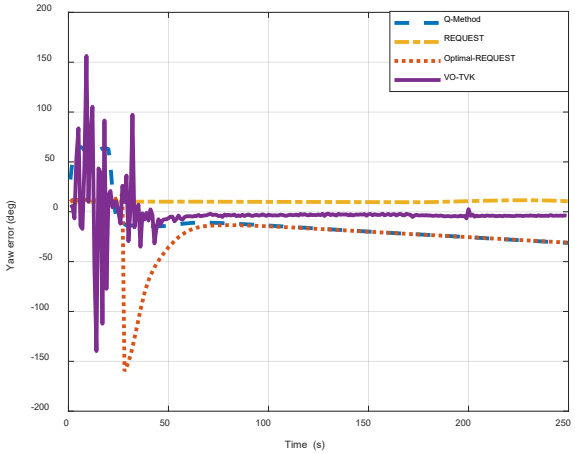

Fig. 7. Curves of yaw angle errors.

To compare algorithms' performances intuitively, each algorithm's attitude errors are listed in Table IV, in which the 'Mean' and 'RMSE' represent the mean and the root mean square error of attitude errors. From the quantitative results of the data, the RMSEs of the three angles calculated by the VO-TVK algorithm are the smallest between 150s and 250s. The comparisons of yaw angle are evident. After the Q-Method and Optimal-REQUEST are stable, the yaw errors are still increased. The obvious reason of this increase is that the Q-Method and Optimal-REQUEST algorithms cannot well alleviate the impacts of the errors included in vector observations, especially the impacts of velocity errors. In addition, although the calculation process of the REQUEST algorithm is very stable, the errors are always large because of the unchanged empirical constant gain. Through the above-mentioned analyses, it can be concluded that the VO-TVK algorithm has better ability to reduce the impacts from vector observations in comparison with the traditional algorithms. Therefore, the VO-TVK algorithm is more suitable for in-motion initial alignment.

TABLE IV

ERROR STATISTICS OF FOUR ALGORITHMS IN SIMULATION TEST

	Items		Q-Method	REQUEST	Optimal-REQUEST	VO-TVK
Pitch (deg)	1~100s	Mean	-1.1914	-0.8872	-1.2569	-1.0679
		RMSE	1.5200	1.1307	1.7184	1.3503
	100~250s	Mean	-0.3755	-0.3204	-0.3702	-0.2435
		RMSE	0.3833	0.3255	0.3784	0.2481
Roll (deg)	1~100s	Mean	-0.6486	-0.0702	-0.7394	0.0221
		RMSE	0.8818	0.6261	0.9142	0.0870
	100~250s	Mean	-0.0569	0.0733	-0.0426	-0.0030
		RMSE	0.3021	0.1201	0.2943	0.0105
Yaw (deg)	1~100s	Mean	-3.5133	9.9815	-22.3781	-0.2471
		RMSE	26.2802	9.9825	40.5657	28.9407
	100~250s	Mean	-25.6217	10.5216	-25.5541	-3.7628
		RMSE	25.8320	10.5488	25.7511	3.8838

B. Vehicle Test

In vehicle test, the effectiveness and superiority of the proposed method are demonstrated more deeply. The SINS, which is combined triaxial closed-loop fiber optic gyroscopes and triaxial micromechanical accelerometers, is equipped to collect raw data. Table V shows the specific parameters of

inertial devices. The GPS receiver produced by the NovAtel is used as the aiding system. Considering that the true attitude angles of the vehicle are unavailable in practical vehicle test, the attitude information collected by high-accuracy SINS is used to provide a reference. The attitude errors of high-accuracy SINS is less than 0.006º for pitch and roll angle and 0.01º for yaw angle. The sampling rates of SINS and GPS Receiver are 200Hz and 1Hz, respectively. Specifically, the SINS is installed on the surface of the steel plate. The vehicle and equipment are shown in Fig. 8, and the whole test lasts for 300s. The vehicle test was carried out in Qingdao City, China. The reference attitudes and the velocities in the vehicle test are presented in Fig. 9 and Fig. 10. The trajectory of the vehicle test is depicted in Fig. 11.

TABLE V

PARAMETERS OF THE IMU IN VEHICLE TEST

Items	Gyroscope
Gyro rate bias (deg/hr)	<1.0
Gyro rate scale factor (ppm)	100
Angular random walk (deg/$\sqrt{\text{hr}}$)	<0.05
Output frequency (Hz)	200
Items	**Accelerometer**
Accelerometer scale factor (ppm)	250
Accelerometer bias (mg)	<1.0
Output frequency (Hz)	200

Fig. 8. Practical test vehicle platform.

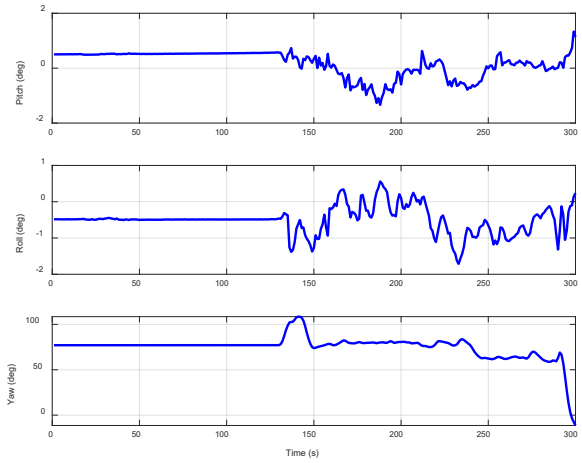

Fig. 9. Reference attitude in the vehicle test.

In this vehicle test, the errors of the pitch, roll and yaw among the four methods are shown in Figs. 12-14, respectively. The blue, yellow, red and purple curves in Figs. 12-14 represent the Q-Method algorithm, the REQUEST algorithm, the Optimal-REQUEST algorithm and the VO-TVK algorithm. In order to compare the alignment errors among four algorithms more specifically, the values of Mean and RMSE are listed in Table VI.

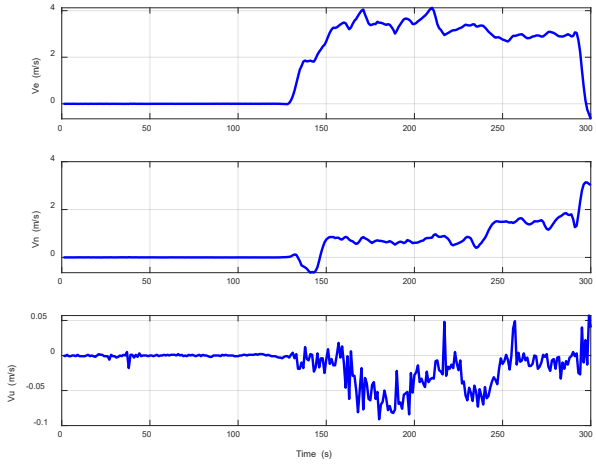

Fig. 10. Reference velocity in the vehicle test.

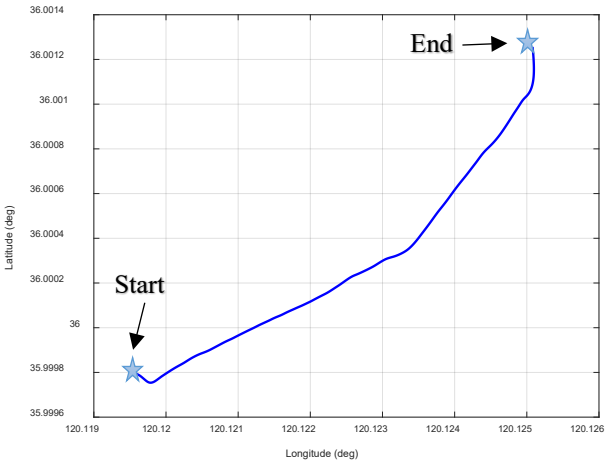

(a) Coordinates of the reference trajectory

(b) Google map of the reference trajectory

Fig. 11 Vehicle trajectory.

It can see from Figs. 12-14, the pitch angle curves and roll angle curves of the four methods are all divergent. This phenomenon does not occur in simulation test, because the accelerometer's constant bias in vehicle test is a hundred times bigger than that in simulation test. The SINS used in the vehicle

This article has been accepted for publication in IEEE Transactions on Instrumentation and Measurement. This is the author's version which has not been fully edited and content may change prior to final publication. Citation information: DOI 10.1109/TIM.2022.3196431

test is made up of fiber optic gyroscopes and micromechanical accelerometers. As is well known, the calculations of pitch and roll angles are dependent on the accuracy of accelerometers, and the huge constant bias of accelerometers will damage the performance of the comparison algorithm and the proposed VO-TVK algorithm. Due to the limitation of the experimental conditions, the outputs of higher-accuracy accelerometer are unavailable. Thus, from Figs. 12-13 and Table VI, it indicates the accuracy of the pitch and roll angles among the Q-Method, the Optimal-REQUEST and the VO-TVK algorithm is approximately equivalent. However, the REQUEST algorithm has large fluctuations in all three angles' results. This phenomenon proves the unreliability of the empirical constant gain. In the actual vehicle test, the REQUEST algorithm is lacking robustness as the empirical constant gain is used to update *K*-matrix. If the constant gain is very small, the old *K*-matrix (calculated in the last time interval) will be very large, which will lead to the REQUEST algorithm cannot accurately calculate the yaw angles. On the contrary, if the empirical constant gain is set small, the REQUEST algorithm will be affected by the cumulative error, resulting in the failure of the algorithm. The proposed VO-TVK solves this problem well, as it use Kalman filtering to update *K*-matrix.

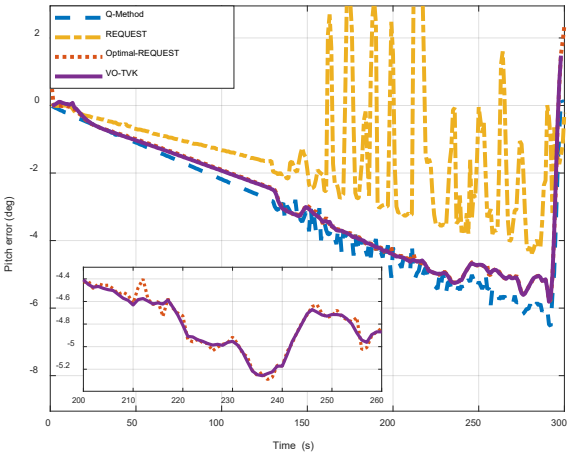

Fig. 12. Curves of pitch errors in the vehicle test.

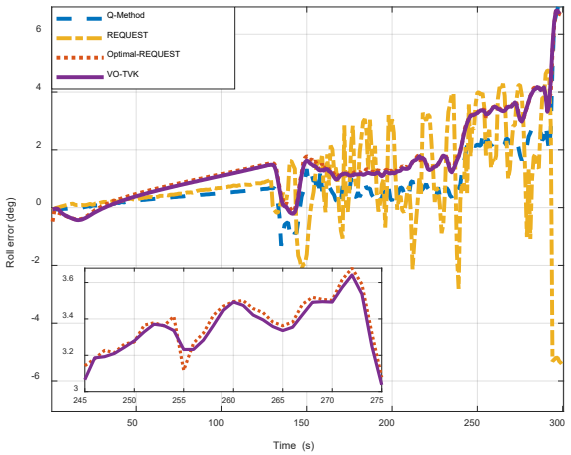

Fig. 13. Curves of roll errors in the vehicle test.

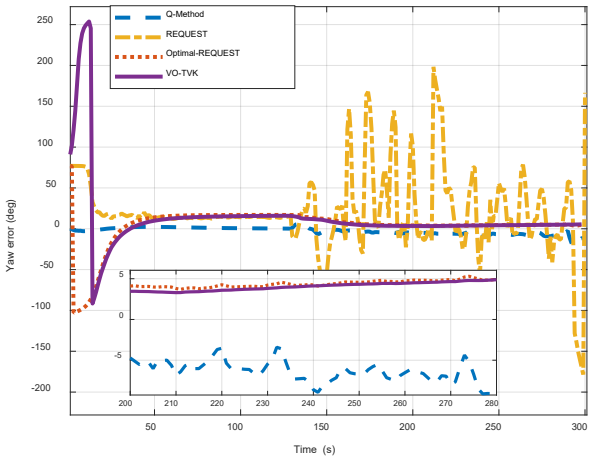

Fig. 14. Curves of yaw errors in the vehicle test.

TABLE VI

ERROR STATISTICS OF FOUR ALGORITHMS IN VEHICLE TEST

	Items		Q-Method	REQUEST	Optimal-REQUEST	VO-TVK
Pitch (deg)	1~150s	Mean	-1.6607	-0.9969	-1.4892	-1.5062
		RMSE	1.9146	1.1545	1.7488	1.7699
	150~300s	Mean	-4.7894	-1.7266	-4.3421	-4.4377
		RMSE	4.9086	2.7363	4.5121	4.5443
Roll (deg)	1~150s	Mean	0.2369	0.3399	0.6284	0.5693
		RMSE	0.4517	0.6590	0.8737	0.8213
	150~300s	Mean	1.4177	1.3314	2.3642	2.2658
		RMSE	1.9453	2.5181	2.7308	2.6174
Yaw (deg)	1~150s	Mean	0.5836	17.5958	1.7077	22.0975
		RMSE	1.8989	29.6687	34.3181	63.8036
	150~300s	Mean	-6.0599	24.9539	5.0449	4.4734
		RMSE	6.9079	68.7321	5.2649	4.6143

Meanwhile, it is evident in Fig. 14 and Table VI that the proposed VO-TVK algorithm has better performance than other compared algorithms in calculating yaw angles. Though the Q-Method has a faster convergence speed than the VO-TVK algorithm, the former algorithm has a weak ability to relieve the errors of vector observation, resulting in the divergence trend of yaw angle error. The REQUEST, Optimal-REQUEST algorithm and the VO-TVK algorithm have a similar convergence rate, which is approximately 50s. However, it is the most precise that the yaw errors calculated by the VO-TVK algorithm. As can be seen from the Table VI, the value of RMSE during 150~300s calculated by the VO-TVK algorithm is approximately reduced by 33% and 12% compared with the Q-Method and the Optimal-REQUEST algorithm, respectively. Through the minimum variance estimation, the VO-TVK overcomes the defect of the conservative estimation performance index used in the Optimal-REQUEST and improves the performance of yaw calculation.

Therefore, the above-mentioned analyses exhibit that the VO-TVK algorithm has better alignment accuracy than the compared algorithms.

C. Lake Trial

In order to further verify the effectiveness of the proposed VO-TVK method when AUV is sailing on the water, a lake trial was conducted in Weishan Lake, China.

This article has been accepted for publication in IEEE Transactions on Instrumentation and Measurement. This is the author's version which has not been fully edited and content may change prior to final publication. Citation information: DOI 10.1109/TIM.2022.3196431

The parameters of inertial measurement units are listed in Table V. The specific models and other parameters of high-accuracy SINS and GPS are described in the Section IV-B. The reference attitudes and the velocities in the lake trial are shown in Fig. 15 and Fig. 16. The trajectory and devices of the trial is shown in Fig. 17, and the entire trial process lasts 300s. Similar to vehicle test, four algorithms are compared in lake trial. The errors of pitch, roll and yaw angles are shown in Figs. 18-20. The results of Mean and RMSE for four algorithms are listed in Table VII. The obvious difference between the lake trial and vehicle test is the velocity of test carrier, but the lake trial environment is closer to the real working one of AUV.

The errors of pitch angle in Fig. 18 are different compared with that in Fig. 12. It is obvious that the REQUEST algorithm has three different performances in the simulation, the vehicle test and the lake trial. This phenomenon means that the selection of empirical constant gain is not reliable and stable. Moreover, the curves of the REQUEST are not smooth enough and they have slight fluctuation when the roll angle has change during 200~220s. The same phenomenon happens in Fig. 19 as well. Therefore, based on the results of the three experiments, the REQUEST algorithm is not the best choice for in-motion coarse alignment. Meanwhile, from the Table VII, it can be seen that, during 200~300s, the RMSE calculated by the VO-TVK algorithm is approximately reduce by 9%, 10% and 5% compared with the Q-Method, the REQUEST and the Optimal-REQUEST algorithm, respectively.

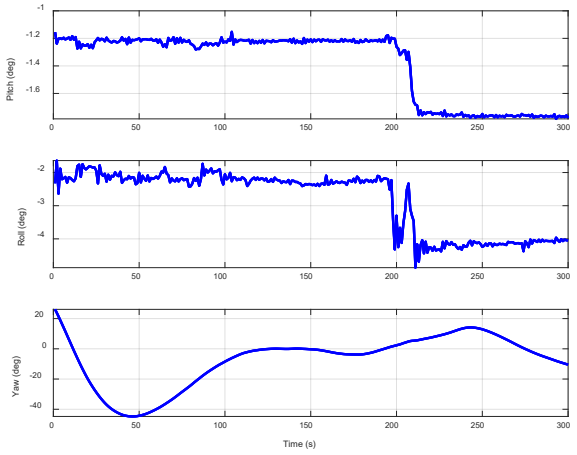

Fig. 15. Reference attitude in the lake trial.

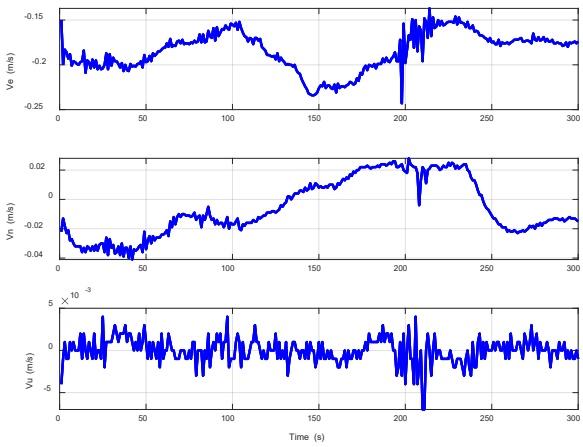

Fig. 16. Reference velocity in the lake trial.

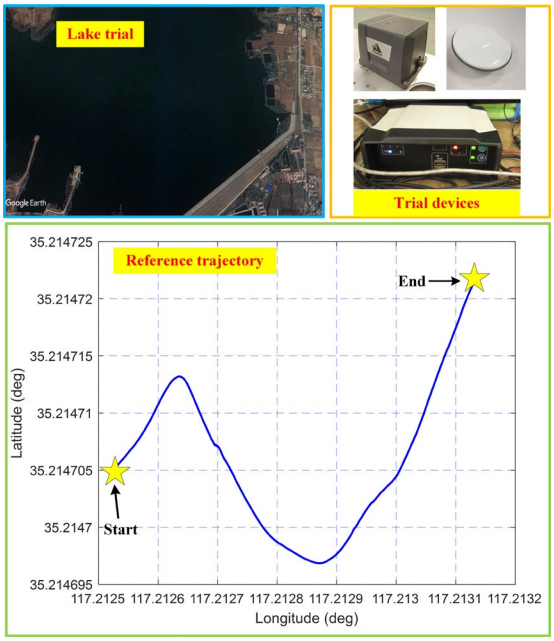

Fig. 17. Lake trial, trial devices and trajectory.

The curves of roll angles in Fig. 19 are also divergent, which are similar to the results in the vehicle test, and the main reason is still the large constant bias of accelerometers. Although among three angles, the errors of roll angles have the most obvious divergence phenomenon, it still can be seen from Fig. 19 that the errors of roll angles calculated by the proposed VO-TVK algorithm are smaller than that of Q-Method and Optimal-REQUEST algorithm.

In Fig. 20, the yaw angles can best verify the merits of the proposed VO-TVK algorithm. It can be observed that the VO-TVK algorithm tends to be stable within 20s, which is the fastest compared with the other three algorithms. Besides, along with the alignment time, errors of vector observation are accumulating resulting in the increase of yaw errors. The VO-TVK obviously has a better ability to suppress the divergent trend than other three algorithms. From Table VII, the RMSEs of yaw errors in 200~300s calculated by the proposed VO-TVK algorithm are approximately reduced by 20%, 70% and 5% compared with the Q-Method, the REQUEST and the Optimal-REQUEST algorithms, respectively.

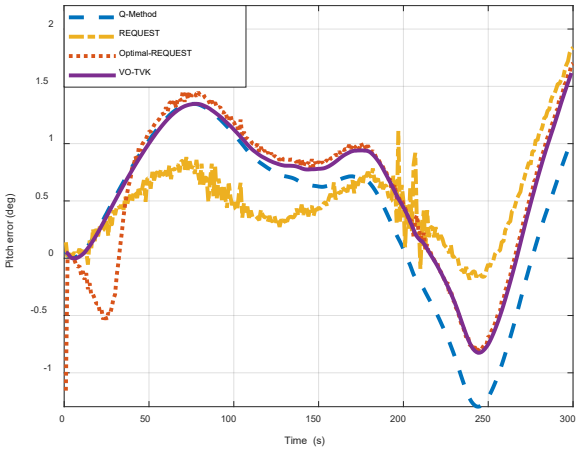

Fig. 18. Curves of pitch errors in the lake trial.

This article has been accepted for publication in IEEE Transactions on Instrumentation and Measurement. This is the author's version which has not been fully edited and content may change prior to final publication. Citation information: DOI 10.1109/TIM.2022.3196431

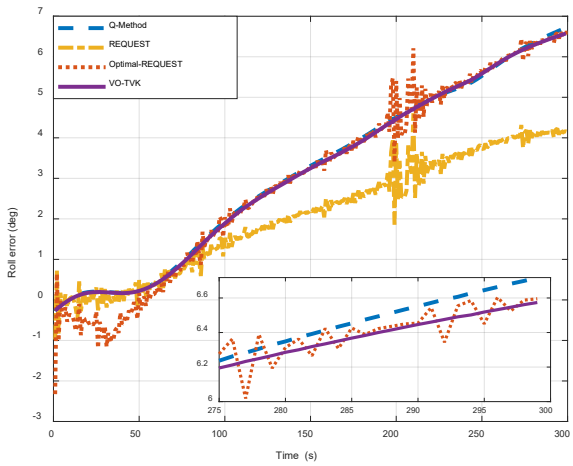

Fig. 19. Curves of roll errors in the lake trial.

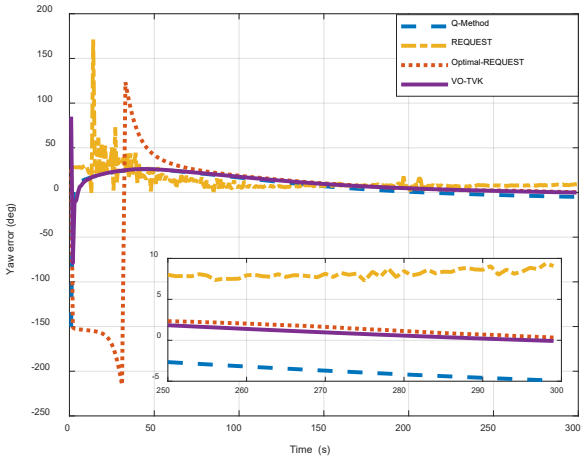

Fig. 20. Curves of yaw errors in the lake trial.

In conclusion, the in-motion coarse alignment method proposed in this paper has more accuracy and faster convergence rate. Therefore, it is more suitable than the compared algorithms to apply to the in-motion coarse alignment.

V. CONCLUSION AND FUTURE WORK

This paper proposes an improved in-motion coarse alignment method with GPS-aided. Firstly, when the AUV is sailing on the ocean, the reference and measurement vectors are changed with the rotation of the Earth and the motion of the vehicle. Thus, the vectors are constructed with the measurements of SINS and GPS. Meanwhile, the discrete forms of the reference and measurement vectors are derived in detail. Secondly, based on vector observation and truncated vectorized *K*-matrix, an in-motion alignment method is devised to suppress the sensors errors and velocity errors contained in the vector observation. The proposed VO-TVK algorithm takes advantages of two complementary approaches for attitude determination, which are the Kalman filtering and the Wahba problem. Finally, the simulation, vehicle test and lake trial are implemented to validate the performance of the proposed algorithm. The results show that the proposed algorithm improves the accuracy and convergence rate of coarse alignment. However, due to the limited conditions, the large constant biases of gyroscopes and accelerometers are not considered here, and the proposed algorithm may have poor performance when using the low-cost MEMS grade SINS to measure. And the error of the first velocity is also ignored in this paper. We will incorporate the constant biases of gyroscopes and accelerometers into the estimation algorithm and consider the error of the first velocity measurement in future works.

TABLE VII

ERROR STATISTICS OF FOUR ALGORITHMS IN LAKE TRIAL

	Items		Q-Method	REQUEST	Optimal-REQUEST	VO-TVK
Pitch (deg)	1~100s	Mean	0.8389	0.5075	0.7080	0.8285
		RMSE	0.9634	0.5716	1.0206	0.9583
	100~200s	Mean	0.6675	0.4981	0.8806	0.8381
		RMSE	0.6952	0.5201	0.8907	0.8471
	200~300s	Mean	-0.3909	0.4896	0.1439	0.0887
		RMSE	0.7625	0.7676	0.7279	0.6898
Roll (deg)	1~100s	Mean	0.5707	0.4105	0.1591	0.5400
		RMSE	0.8171	0.6529	0.9029	0.7847
	100~200s	Mean	3.2951	2.1982	3.2691	3.2345
		RMSE	3.3705	2.2549	3.3580	3.3101
	200~300s	Mean	5.6100	3.7050	5.6329	5.5982
		RMSE	5.6488	3.7319	5.6734	5.6333
Yaw (deg)	1~100s	Mean	19.2401	21.3042	-23.5243	20.6257
		RMSE	19.2401	21.3042	-23.5243	20.6257
	100~200s	Mean	7.5769	7.5945	10.6507	10.0324
		RMSE	8.8929	7.7739	11.4023	10.7134
	200~300s	Mean	-2.4859	7.7692	2.2504	1.9619
		RMSE	2.9748	7.9664	2.5241	2.3798

APPENDIX A

The frames used in this paper are defined as below and Fig. 21 illustrates the coordinate frames.

1) *i*-frame: Earth-centered initially-fixed orthogonal reference frame;
2) *n*-frame: Orthogonal reference frame aligned with East-North-Up (ENU) geodetic axes;
3) *b*-frame: Right-forward-upper orthogonal reference frame aligned with inertial measurement unit axes;
4) *b*0-frame: Orthogonal reference frame that is non-rotating relative to the *i*-frame, which is formed by fixing the *b*-frame at start-up in the inertial space

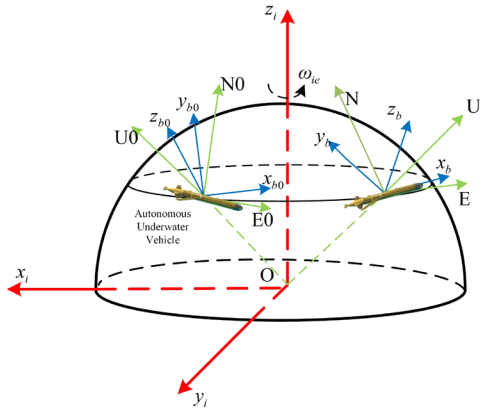

Fig. 21. Definition of the coordinate frames.

APPENDIX B

The illation of $\mathbf{v}_{k+1}^{n}$ in Eq. (46) will be introduced in this section.

Assuming a batch of vector observations are acquired simultaneously at the time of t_{k+1}, the measurement equation of the *K*-matrix can be written as:

$$\delta\mathbf{K}_{k+1}=\mathbf{K}_{k+1}+\mathbf{V}_{k+1}^{n} \tag{65}$$

where $\mathbf{V}_{k+1}^{n}$ denotes the global measurement error in $\delta\mathbf{K}_{k+1}$.

Next, to derive the expression conveniently, $\mathbf{B}_{\mu}^{n}$ is defined as:

$$\mathbf{B}_{\mu}^{n}=\sum_{i=1}^{n}a_i\delta\boldsymbol{\mu}_{k+1}^{i}(\mathbf{r}_{k+1}^{i})^{\mathrm{T}} \tag{66}$$

where $\delta\boldsymbol{\mu}_{k+1}^{i}$ is the measurement error in the i^{th} observation, $\sum_{i=1}^{n}a_i=1$.

Each single observation is defined 3×3 matrix $\mathbf{B}_{\mu_i}$ ($i=1,2\cdots,n$):

$$\mathbf{B}_{\mu_i}\triangleq\delta\boldsymbol{\mu}_{k+1}^{i}(\mathbf{r}_{k+1}^{i})^{\mathrm{T}} \tag{67}$$

Substituting Eq. (63) into Eq. (62) yields:

$$\mathbf{B}_{\mu}^{n}=\sum_{i=1}^{n}a_i\mathbf{B}_{\mu_i} \tag{68}$$

$\mathbf{V}_{k+1}^{i}$ for each single observation can be expressed as:

$$\mathbf{V}_{k+1}^{i}=\begin{bmatrix}\mathbf{S}_{\mu}^{i}-\sigma_{\mu}^{i}\mathbf{I}_3 & \mathbf{z}_{\mu}^{i}\\ (\mathbf{z}_{\mu}^{i})^{\mathrm{T}} & \sigma_{\mu}^{i}\end{bmatrix} \tag{69}$$

Similarly to the matrix $\mathbf{B}_{\mu_i}$, the measurement matrix global error $\mathbf{V}_{k+1}^{n}$ can be calculated as:

$$\mathbf{V}_{k+1}^{n}=\sum_{i=1}^{n}a_i\mathbf{V}_{k+1}^{i} \tag{70}$$

After that, the vector $\mathbf{v}_{k+1}^{i}$ can be truncated and vectorized as follows:

$$\mathbf{v}_{k+1}^{i}=[\begin{matrix}V_{k+1_{11}}^{i} & V_{k+1_{12}}^{i} & V_{k+1_{13}}^{i} & V_{k+1_{14}}^{i} & V_{k+1_{22}}^{i}\\ V_{k+1_{23}}^{i} & V_{k+1_{24}}^{i} & V_{k+1_{33}}^{i} & V_{k+1_{34}}^{i}\end{matrix}]^{\mathrm{T}} \tag{71}$$

Then, use $\mathbf{v}_{k+1}^{i}$ instead of $\mathbf{V}_{k+1}^{i}$ to define the matrix $\mathbf{v}_{k+1}^{n}$. According to Eq. (66), $\mathbf{v}_{k+1}^{n}$ can be written as follows:

$$\mathbf{v}_{k+1}^{n}=\sum_{i=1}^{n}a_i\mathbf{v}_{k+1}^{i} \tag{72}$$

Considering that $\mathbf{v}_{k+1}^{i}$ is the measurement error associated with each single observation, $\mathbf{r}_{k+1}^{i}$ can be substituted for $\mathbf{r}_{k+1}$ into Eq. (47). $\boldsymbol{\Lambda}_{k+1}^{i}$ denotes the sequence of the n single output gain matrices ($i=1,2,\cdots,n$). Then, the following equation can be acquired:

$$\mathbf{v}_{k+1}^{i}=\boldsymbol{\Lambda}_{k+1}^{i}\delta\boldsymbol{\mu}_{k+1}^{i} \tag{73}$$

Substituting Eq. (66) into Eq. (65) yields the sought equation of $\mathbf{v}_{k+1}^{n}$, as shown in Eq. (46).

APPENDIX C

In this section, the zero-trace characteristic of *K*-matrix is shown as below.

The calculation of *K*-matrix's trace can be written as:

$$\begin{aligned}&tr\left(\mathbf{S}_{k+1}-\sigma_{k+1}\mathbf{I}_3\right)+\sigma_{k+1}\\&=tr(\mathbf{S}_{k+1})-tr(\sigma_{k+1}\mathbf{I}_3)+\sigma_{k+1}\end{aligned} \tag{74}$$

Combing the Eqs. (40) and (42), we can acquire the result of the trace.

$$\begin{aligned}&tr(\mathbf{S}_{k+1})-tr(\sigma_{k+1}\mathbf{I}_3)+\sigma_{k+1}\\&=tr\left(\mathbf{B}_{k+1}\right)+tr\left(\mathbf{B}_{k+1}^{T}\right)-\sigma_{k+1}tr(\mathbf{I}_3)+\sigma_{k+1}\\&=\sigma_{k+1}+\sigma_{k+1}-3\sigma_{k+1}+\sigma_{k+1}=0\end{aligned} \tag{75}$$

After vectorization, the zero trace property of *K*-matrix can be expressed by the Eq.(63) combined with the Eq. (64).

ACKNOWLEDGMENT

This work is supported by the Natural Science Foundation of Jiangsu Province (BK20221500), the National Natural Science Foundation of China (61703098), and the Fujian Provincial Key Laboratory of Coast and Island Management Technology Study (FJCIMTS2019-03). This work is also supported in part by London Tech Bridge, the APEX Undersea Challenge, the European Regional Development Fund—Industrial Intensive Innovation Programme, the Research Fund from the Science and Technology on Underwater Vehicle Technology Laboratory (2021JCJQ-SYSJJ-LB06905), and the Water Science and Technology Project of Jiangsu Province under grant (2021072, 2021063).

REFERENCES

[1] C. C. Eriksen, T. J. Osse, and R. D. Light, "Seaglider: a long-range autonomous underwater vehicle for oceanographic research," *IEEE Journal of Oceanic Engineering*, vol. 26, no. 4, pp. 424-436, 2001.

[2] S. Gao, B. He, X. Zhang, J. H. Wan, X. K. Mu, and T. H. Yan, "Cruise speed estimation strategy based on multiple fuzzy logic and extended state observer for low-cost AUV," *IEEE Transactions on Instrumentation and Measurement*, vol. 70, pp. 1-13, 2020.

[3] L. Paull, S. Saeedi, M. Seto, and H. Li, "AUV navigation and localization: A review," *IEEE Journal of Oceanic Engineering*, vol. 39, no. 1, pp. 131–149, 2014.

[4] H. Q. Huang, J. C. Tang, C. Liu, B. Zhang, and B. Wang, "Variational Bayesian-Based filter for inaccurate input in underwater navigation," *IEEE Transactions on Vehicular Technology*, vol. 70, no. 9, pp. 8441-8452, 2021.

[5] P. A. Miller, J. A. Farrell, Y. Zhao, and V. Djapic, "Autonomous underwater vehicle navigation," *IEEE Journal of Oceanic Engineering*, vol. 35, no. 3,pp. 663–678, 2010.

[6] H. Q. Huang, J. C. Tang, R. Song, and X. H. Tang, "A novel matrix block algorithm based on cubature transformation fusing variational Bayesian scheme for position estimation applied to MEMS navigation system," *Mechanical Systems and Signal Processing*, vol. 166, no. 108486, 2022.

[7] T. Sands, "Development of deterministic artificial intelligence for unmanned underwater vehicles (UUV)," *Journal of Marine Science and Engineering*, vol. 8, no.8, 2020.

[8] D. Wang, X. S. Xu, Y. Q. Yao, T, Zhang, and Y. Y. Zhu, "A novel SINS/DVL tightly integrated navigation method for complex environment," *IEEE Transactions on Instrumentation and Measurement*, vol. 69, no. 7, pp. 5183-5196, 2020.

[9] H. Ahmed, and M. Tahir, "Accurate attitude estimation of a moving land vehicle using low-cost MEMS IMU sensors," *IEEE Transactions on Intelligent Transportation Systems*, vol. 18, no. 7, pp. 1723-1739, 2017.

[10] D. Wang, X. S. Xu, Y. Yang, and T. Zhang, "A Quasi-Newton quaternions calibration method for DVL error aided GNSS," *IEEE*

Transactions on Vehicular Technology, vol. 70, no. 3, pp. 2465-2477, 2021.

[11] P. M. G. Silson, "Coarse alignment of a ship's strapdown inertial attitude reference system using velocity loci," *IEEE Transactions on Instrumentation and Measurement*, vol. 60, pp. 1930-1941, 2011.

[12] H. Q. Huang, J. C. Tang, M. Y. Wang, B. Wang, and X. F. He, "A novel partitioned matrix-based parameter update method embedded in Variational Bayesian for underwater positioning," *IET Control Theory and Applications*, vol. 14, no. 4, 2022.

[13] X. Xu, Y. Sun, J. Gui, Y. Yao, and T. Zhang, "A fast robust in-motion alignment method for SINS with DVL aided," *IEEE Transactions on Vehicular Technology*, vol. 69, no. 4, pp. 3816-3827, 2020.

[14] J. N. Xu, H. Y. He, F. J. Qin, and L. B. Chang, "A novel autonomous initial alignment method for strapdown inertial navigation system," *IEEE Transactions on Instrumentation and Measurement*, vol. 66, no. 9, pp. 2274-2282, 2017.

[15] L. B. Chang, J. S. Li, and S. Y. Chen, "Initial alignment by attitude estimation for strapdown inertial navigation systems," *IEEE Transactions on Instrumentation and Measurement*, vol. 64, no. 3, pp. 784-794, 2015.

[16] C. M Tan, X. H. Zhu, Y. Sun, Y. Wang, Z. Q. Wu, and D. B. Gu, "A new analytic alignment method for a SINS," *Sensors*, vol. 15, no. 11, pp. 27930-27953, 2015.

[17] X. Xu, X. S Xu, T. Zhang, Y. Li, and J. W. Tong, "A Kalman filter for SINS self-alignment based on vector observation," *Sensors*, vol. 17, no.2, 2017.

[18] M. P. Wu, Y. X. Wu, X. P. Hu, and D. W. Hu, "Optimization-based alignment for inertial navigation systems: Theory and algorithm," *Aerospace Science and Technology*, vol. 15, pp. 1-17, 2011.

[19] Y. X. Wu, and X. F. Pan, "Velocity/Position integration formula part I: Application to in-flight coarse alignment," *IEEE Transactions on Aerospace and Electronic System*, vol. 49, no. 2, pp. 1006-1023, 2013.

[20] Y. X. Wu, and X. F. Pan, "Velocity/Position integration formula part II: Application to strapdown inertial navigation computation," *IEEE Transactions on Aerospace and Electronic System*, vol. 49, no. 2, pp. 1024-1034, 2013.

[21] R. Koja, "On methods for in-flight alignment of inertial navigation systems," Master Dissertation, Engineering and Space Tecnoloy, Brazil, Feb. 2019.

[22] M. D. Shuster, "Filter quest or request," *Journal of guidance, Control and Dynamics*, vol. 32, no. 2, pp. 643-645, 2009.

[23] X. Xu, X. S. Xu, T. Zhang, and Z. C. Wang, "In-motion Filter-QUEST alignment for strapdown inertial navigation systems," *IEEE Transactions on Instrumentation and Measurement*, vol. 67, no. 8, pp. 1979-1993, 2018.

[24] Y. Y. Zhu, T. Zhang, and X. Xu, "A coarse-alignment method based on the Optimal-REQUEST algorithm," *Sensors*, vol. 18, no. 239, 2018.

[25] T. Zhang, Y. Y. Zhu, X. Xu, J. Wang, and Y. Li, "In-motion coarse alignment based on the vector observation for SINS," *IEEE Transactions on Instrumentation and Measurement*, vol. 68, no. 10, pp. 3740-3750, 2019.

[26] D. Choukroun, "Quaternion estimation using Kalman filtering of the vectorized K-matrix," *AIAA Guidance, Navigation, and Control Conference*, Chicago, 2009.

[27] J. Keat, "Analysis of least-squares attitude determination routine, DOAOP," *Computer Sciences Crop.*, Report CSC/TM-77/6034, 1977.

[28] X. Xu, J. Gui, Y. F. Sun, Y. Q. Yao, and T. Zhang, "A robust in-motion alignment method with inertial sensors and Doppler velocity log," *IEEE Transactions on Instrumentation and Measurement*, vol. 70, pp. 1-13, 2021.

[29] Y. Q. Yao, X. S. Xu, Y. Y. Zhu, and X. Xu, "In-motion coarse alignment method for SINS/DVL with the attitude dynamics," *ISA Transactions*, vol. 105, pp. 377-386, 2020.

[30] Y. L. Huang, Z. Zhang, S. Y. Du, Y. F. Li, and Y. G. Zhang, "A high-accuracy GPS-aided coarse alignment method for MEMS-based SINS," *IEEE Transactions on Instrumentation and Measurement*, vol. 69, no. 10, pp. 7914-7932, 2020.

[31] Y. L. Huang, Y. G. Zhang, and L. B. Chang, "A new fast in-motion coarse alignment method for GPS-aided low-cost SINS," *IEEE/ASME Transactions on Mechatronics*, vol. 23, no. 3, pp. 1303-1313, 2018.

[32] L. B. Chang, J. S. Li, and K. L. Li, "Optimization-based alignment for strapdown inertial navigation system: Comparison and extension," *IEEE Transactions on Aerospace and Electronic Systems*, vol. 52, no. 4, pp. 1697-1713, 2016.

[33] R. Koja, and W. de. C. L. Filho, "Revisited position-velocity integration formulas for in-flight self-alignment of GPS-aided inertial navigation systems," Brazilian Conf. Dyn. 2017.

Haoqian Huang (M'18) received the Bachelor degree in automation from the China University of Mining and Technology, China, in 2007, the Master degree in agricultural mechanization engineering from Nanjing Agricultural University, China, in 2010, and the Ph.D. degree in instrument science and technology from Southeast University, China, 2015. From 2015 to 2017, he was a PostDoctoral Researcher with Southeast University. He then joined Hohai University, China, where he is currently an Associate Professor with College of Energy and Electrical Engineering, Hohai University since 2017. His main research interests include navigation technology applied to underwater vehicle, inertial navigation, information fusion and so on. He received the first prize at China General Chamber of Commerce Science and Technology Award, the second prize at China Machinery Industry Science and Technology Award, the third prize at Jiangsu University Science and Technology Research Achievement Award, and Bronze Medal at the 43th Geneva International Exhibition of Inventions for his Underwater Navigation System Design. He has served as a lead Guest Editor of Special Issue in *Mathematical Problems in Engineering*, and Guest Editor of Special Issue in *Applied Sciences*.

Jiaying Wei was born in Nanjing, Jiangsu, China, in 1998. She received the B. S. degree from Nanjing Tech University, Nanjing, China, in 2020. She is currently pursuing the M. S. degree in control theory and control engineering from the Hohai University, China. Her current research interests include inertial navigation, initial alignment, and MEMS inertial technology.

Di Wang received the B.S. degree in electronic science and technology from Jiangsu Normal University, Xuzhou, Jiangsu, in 2015, and the M.S. degree in control science and engineering from Lanzhou Jiaotong University, Lanzhou, Gansu, China, in 2018. He is currently pursuing the Ph.D. degree in navigation, guidance, and control with Southeast University, Nanjing. His research interests include inertial navigation and integrated navigation technology, underwater navigation algorithms, and SINS/DVL integrated algorithms, which is applied in the field of underwater navigation technology.

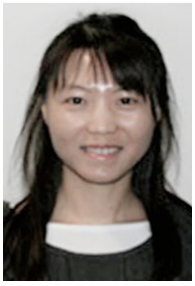

Li Zhang (Senior Member, IEEE) received the Ph.D. degree from the University of Birmingham. She is a Reader of computer science in Royal Holloway, University of London, UK. Previously she was a Professor in National Subsea Centre, Aberdeen, UK, and an Associate Professor (Reader) of computer science with Northumbria University, U.K. She is also working as an Honorary Research Fellow with the University of Birmingham. She holds expertise in machine learning, deep learning, and evolutionary computation. She has served as an Associate Editor for Decision Support Systems.

Bing Wang (Member, IEEE) received the B.S. degree from the Department of Automatic Control, Huazhong University of Science and Technology (HUST), in 1998, and the Ph.D degree from the Department of Automation, University of Science and Technology of China (USTC), in 2006. He is currently a Professor in the College of Energy and Electrical Engineering, Hohai University. His research interests include nonlinear multiagent systems, wind power generation, artificial intelligence.